Chromosome 1q amplification perturbs a ceRNA network to promote melanoma metastasis

Xiaonan Xu[1], Kaizhen Wang[1], Olga Vera[1], Akanksha Verma[2], Olivier Elemento[2], Xiaoqing Yu[3], Florian A. Karreth[1,4,#]

[1] Department of Molecular Oncology, H. Lee Moffitt Cancer Center and Research Institute, Tampa, Florida 33612, USA

[2] Caryl and Israel Englander Institute for Precision Medicine, Institute for Computational Biomedicine, Department of Physiology and Biophysics, Weill Cornell Medicine, New York, NY, 10065, USA

[3] Department of Biostatistics and Bioinformatics, H. Lee Moffitt Cancer Center and Research Institute, Tampa, Florida 33612, USA

[4] Lead contact

[#] Correspondence: Florian.Karreth@moffitt.org (F.A.K.)

Running title: A ceRNA network promotes melanoma metastasis

Keywords: ceRNA, miRNA, melanoma, metastasis, CEP170, NUCKS1, ZC3H11A, chromosome 1q amplification

SUMMARY

Deregulated gene expression through epigenetic, transcriptional, and copy number alterations is a major driver of melanoma progression and metastasis. In addition to serving as blueprints for translation, some mRNAs post-transcriptionally regulate gene expression by competitively sequestering miRNAs they share with other targets. Here we report that such mRNAs, termed competitive endogenous RNAs (ceRNAs), contribute to melanoma progression and metastasis. ceRNA predictions identified multiple candidate genes on chromosome 1q, which is recurrently amplified in melanoma. Genetic studies reveal that three of these mRNAs, *CEP170*, *NUCKS1*, and *ZC3H11A*, promote melanoma migration, invasion, and metastasis in a protein coding-independent and miRNA binding site-dependent manner. Interestingly, *CEP170*, *NUCKS1*, and *ZC3H11A* cooperate to elicit oncogenic effects by collectively impairing the tumor suppressor activity of 8 miRNAs on several pro-metastatic target genes. Finally, this complex chromosome 1q ceRNA network is evident in other cancer types, suggesting ceRNA network deregulation is a common driver of cancer progression.

INTRODUCTION

Malignant melanoma remains the leading cause of skin cancer-related deaths, almost invariably due to metastases to vital organs. Accordingly, significant efforts have focused on understanding drivers of melanoma progression and metastasis. While genetic events affecting oncogenes and tumor suppressors such as BRAF, NRAS, CDKN2A, and PTEN are well-documented drivers of melanoma development, surprisingly few metastasis-specific mutations have been discovered (Shain et al., 2018; Vogelstein et al., 2013). Indeed, mutations and pathways thus far implicated in melanoma metastasis are those that also promote the early stages of the disease (Damsky et al., 2014; Orgaz and Sanz-Moreno, 2013; Turner et al., 2018), as seen in investigations of autochthonous melanoma models (Ackermann et al., 2005; Cho et al., 2015; Damsky et al., 2011; Dankort et al., 2009; Otsuka et al., 1998; Zingg et al., 2018). It is therefore probable that gene expression changes controlled by epigenetic, transcriptional, post-transcriptional, and/or copy number alterations are drivers of melanoma metastasis (Chatterjee et al., 2018; Ell and Kang, 2013); (Kapoor et al., 2010; Karras et al., 2019; Marie et al., 2020; Pencheva et al., 2012; Shain et al., 2018; Wurth et al., 2016; Zingg et al., 2018).

A more recently validated mechanism that controls gene expression is that mediated by competitive endogenous RNAs (ceRNAs) that function as natural microRNA (miRNA) sponges. Specifically, ceRNAs competitively bind to miRNAs to impair their repressive activity towards their targets (i.e., ceRNA effectors) (Salmena et al., 2011; Tay et al., 2014). Originally described for pseudogenes (Karreth et al., 2015; Poliseno et al., 2010), ceRNA activity has also been observed for dozens of long noncoding RNAs (lncRNAs) and circular RNAs (circRNAs). Interestingly, protein-coding messenger RNAs (mRNAs), typically thought of as the targets of miRNAs, can also act as ceRNAs to promote cancer (Karreth and Pandolfi, 2013). For example, in neuroblastoma the *MYCN* gene is frequently amplified and highly overexpressed, thereby impairing the activity of the tumor suppressor let-7 miRNA family via two let-7 miRNA binding sites in the *MYCN* 3'UTR (Powers et al., 2016). Further, a large ceRNA network in glioblastoma

comprised of 13 mRNAs regulates the expression of PTEN via a miRNA sponging-mediated mechanism (Sumazin et al., 2011), and control of PTEN has also been reported in prostate cancer by the *VAPA* and *CNOT6L* mRNAs (Tay et al., 2011) and in melanoma by the *ZEB2* mRNA (Karreth et al., 2011). Finally, the *TYRP1* mRNA encoding the pigmentation Tyrosinase-related protein 1, promotes melanoma cell proliferation and xenograft growth by sequestering the tumor suppressor miRNA miR-16 via a non-canonical binding site (Gilot et al., 2017).

Collectively, these studies support the notion that mRNAs can function as ceRNAs to regulate gene expression, yet it is not clear if ceRNA activity is a widespread phenomenon nor if mRNAs operate as miRNA sponges only when meeting certain criteria. Similarly, it remains to be determined if ceRNA regulation converges on just a few effectors having prominent oncogenic or tumor suppressor activity such as PTEN (Karreth et al., 2011; Sumazin et al., 2011; Tay et al., 2011). Here we report that a ceRNA network driven by three co-amplified genes, *CEP170*, *NUCKS1*, and *ZC3H11A*, whose mRNAs promote melanoma cell migration, invasion, and metastasis by simultaneously inhibiting 8 tumor suppressive miRNAs to enhance the expression of pro-metastatic genes. Notably *CEP170*, *NUCKS1*, and *ZC3H11A* are co-amplified in several cancers where their expression correlates with upregulation of pro-metastatic ceRNA effectors, suggesting this novel and potent ceRNA network plays oncogenic roles across cancer types.

RESULTS

Amplification and overexpression of 1q ceRNA genes is associated with melanoma metastasis

We hypothesized that genomic amplifications promote melanoma metastasis, at least in part, via overexpression of oncogenic ceRNAs. To identify amplified genes with putative ceRNA potential, we analyzed a TCGA Skin Cutaneous Melanoma dataset containing 366 metastatic

melanoma cases. Given that increasingly amplified and highly expressed genes likely elicit prominent ceRNA effects by contributing a large number of miRNA binding sites to their ceRNA networks, we first identified genes as recurrently amplified in ≥3% of cases and focused on the top 20% highest expressed genes. This analysis yielded 211 candidate genes (**Table S1**). To define putative ceRNA networks we calculated the correlation of the 211 amplified candidate genes with the protein-coding transcriptome (20,291 transcripts). We identified 34,285 significant gene pairs with FDR <0.05 and Spearman correlation ≥0.5. These gene pairs were then tested for enrichment of known miRNA binding sites based on TargetScan algorithm predictions (release 7.2) (Agarwal et al., 2015). To capture highly conserved binding sites for the miRNA families (i.e. miRNA Response Elements, MRE), we used the aggregate P_{CT} score (Friedman et al., 2009) with cut-off of ≥0.2 for every predicted miRNA as a stringent probability metric for conserved targeting (**Table S2**). Out of 34,285 gene pairs, 2,515 gene pairs share at least 4 MREs in their 3'UTRs (**Table S3**) and could thus constitute a complex ceRNA network encompassing 40 amplified putative ceRNAs and 971 effector transcripts (**Figure 1A**). The number of effectors for each ceRNA ranged from 1-454 transcripts, with 9 ceRNAs engaging over 100 effectors (**Figure 1B**).

To further systematically prioritize candidate ceRNAs, we evaluated the connectivity of ceRNA nodes in the network using the Hyperlink-Induced Topic Search (HITS) algorithm (**Figure S1A**), which revealed the top 5 highly ranked putative ceRNA genes located on chromosome 1q (**Table S4**). This raised the possibility of co-amplified ceRNA genes coordinately regulating the same effectors. Indeed, ceRNA genes located within a genomic region connect to similar effectors, with the greatest number of shared effectors observed for chromosome 1q ceRNAs (**Figure S1B**). Among ceRNA genes localized in the chromosome 1q amplicon ($1q^{AMP}$ ceRNAs), *AKT3*, *NUCKS1*, *HNRNPU*, *ZC3H11A*, and *CEP170* showed the greatest number of total and shared effectors (**Figure S1C**).

This ceRNA prediction was based on annotated full-length 3'UTRs. However, alternative polyadenylation (APA) can shorten 3'UTRs and thereby limit their ability to sequester miRNAs. Using data from the APAatlas (https://hanlab.uth.edu/apa/) (Hong et al., 2019), we assessed the prevalence of APA across several tissue types for *AKT3*, *NUCKS1*, *HNRNPU*, *ZC3H11A*, and *CEP170*. This analysis revealed almost universal APA for *HNRNPU*, a wide range of polyA site usage for *NUCKS1*, and predominant usage of canonical polyA sites for *AKT3*, *ZC3H11A*, and *CEP170* (**Figure S1D**). Given shortened 3'UTRs for *HNRNPU* transcripts, this mRNA was excluded from further analyses. Moreover, there were no significant biological effects of ectopic expression of the 3'UTR or coding sequence of *AKT3* on two human melanoma cell lines (**Figure S1E-G**). Accordingly, the $1q^{AMP}$ ceRNAs *CEP170*, *NUCKS1*, and *ZC3H11A* were assessed for their roles in melanoma.

Chromosome 1q amplification correlates with melanoma stage and occurs in over 25% of metastatic melanoma (Bastian et al., 1998; Fountain et al., 1990; Mertens et al., 1997; Thompson et al., 1995). Accordingly, analysis of a TCGA Skin Cutaneous Melanoma dataset revealed the $1q^{AMP}$ ceRNA genes *CEP170*, *NUCKS1*, and *ZC3H11A* show co-occurrence of copy number gains or amplification in approximately 52% (191 out of 367) of metastatic melanoma cases (**Figure 1C**). Further, copy number gains of chromosome 1q are associated with increased expression of *CEP170*, *NUCKS1*, and *ZC3H11A* (**Figure S1H**) and the expression levels of these 3 genes are significantly correlated (**Figure 1D**). Expression of *CEP170*, *NUCKS1*, and *ZC3H11A* is also significantly increased in metastases compared to primary melanomas (**Figure 1E**). In accord with these findings, Gene set enrichment analysis revealed that *CEP170* and *NUCKS1* expression is associated with a metastasis signature, and that *ZC3H11A* exhibited a trend towards association with the metastasis signature (**Figure 1F**). Thus, copy number gains and overexpression of the putative $1q^{AMP}$ ceRNAs *CEP170*, *NUCKS1*, and *ZC3H11A* is associated with melanoma metastasis.

1q^{AMP} ceRNAs have oncogenic effects in melanoma cells in vitro

To assess the functional potential of *CEP170*, *NUCKS1*, and *ZC3H11A* as ceRNAs, we tested if forced overexpression of their 3'UTRs impacts the phenotype of human melanoma cells. Lentiviruses were generated that express the 3'UTRs of *CEP170*, *NUCKS1*, and *ZC3H11A* linked to a GFP cDNA to prevent nonsense-mediated decay, ensure proper folding of the 3'UTRs, and enable tracing of cells expressing the 3'UTRs. Ectopic expression of these constructs in the human melanoma cell lines A375 and WM793 that lack chromosome 1q amplification resulted in 10-40-fold overexpression of the *CEP170*, *NUCKS1*, and *ZC3H11A* 3'UTRs (**Figure S2A**). While overexpression of the *CEP170*, *NUCKS1*, or *ZC3H11A* 3'UTRs had only modest effects on melanoma cell proliferation (**Figure S2B and S2C**), there were marked increases in colony number and size under anchorage-independent conditions in soft agar (Figure 2A). Further, overexpression of these 3'UTRs also enhanced melanoma cell migration and invasion in transwell assays (**Figure 2B and 2C**). Notably, combined overexpression of the *CEP170*, *NUCKS1*, and *ZC3H11A* 3'UTRs further increased anchorage-independent growth, migration, and invasion (**Figure 2A-C**), suggesting cooperative effects of these ceRNAs.

To affirm the oncogenic potential of 1q^{AMP} ceRNAs, shRNAs were used to silence endogenous *CEP170*, *NUCKS1*, or *ZC3H11A* expression in metastatic 1205Lu human melanoma cells (**Figure S2D**). Reduced expression of endogenous *CEP170*, *NUCKS1*, or *ZC3H11A* impaired anchorage-independent growth in soft agar, migration and invasion of 1205Lu cells (**Figure 2D-F**). To test if these effects were mediated by the encoded CEP170, NUCKS1, and ZC3H11A proteins, we also overexpressed the coding sequences (CDS) of the 1q^{AMP} ceRNA genes in A375 and WM793 cells. Strikingly, the CEP170, NUCKS1, and ZC3H11A CDS had no effect on growth in soft agar or on transwell migration and invasion (**Figure S2E and 2F**). Thus, *CEP170*, *NUCKS1*, and *ZC3H11A* augment aggressive melanoma cell phenotypes in vitro in a 3'UTR-dependent but protein coding-independent manner.

1q^{AMP} ceRNAs augment melanoma metastasis in vivo

To test the role of the 3'UTRs of *CEP170*, *NUCKS1*, and *ZC3H11A* in promoting melanoma metastasis, A375 and WM793 melanoma cells harboring luciferase were engineered to express the ectopic *CEP170*, *NUCKS1*, and *ZC3H11A* 3'UTRs. A375 cells were subcutaneously injected into the flanks of NSG mice for spontaneous metastasis assays, while WM793 cells were intravenously inoculated into the tail veins of NSG mice. Notably, bioluminescence imaging revealed that overexpression of the *CEP170*, *NUCKS1*, and *ZC3H11A* 3'UTRs significantly increased tumor burden in the lungs in both the A375 and WM793 metastasis models (**Figures 3A, 3B, S3A, and S3B**). H&E staining corroborated the increased lung metastasis burden upon 1q^{AMP} ceRNA overexpression (**Figure S3C and S3D**). While combined overexpression of the *CEP170*, *NUCKS1*, and *ZC3H11A* 3'UTRs also enhanced lung metastasis, the effect was comparable to overexpression of individual 3'UTRs. Finally, silencing of *CEP170*, *NUCKS1*, or *ZC3H11A* in luciferase-expressing 1205Lu melanoma cells significantly impaired their lung metastatic potential in intravenously inoculated in NSG mice (**Figure 3C, S3E, and S3F**). Thus, 1q^{AMP} ceRNAs promote the metastatic program of melanoma cells.

ceRNA network predictions are based on miRNAs conserved among vertebrates, and the sequence of the 3'UTRs of human and mouse *CEP170*, *NUCKS1*, and *ZC3H11A* have approximately 80% homology, suggesting human 1q^{AMP} ceRNAs may regulate similar networks in human and mouse cells. To test this, we assessed if overexpression of human *CEP170*, *NUCKS1*, and *ZC3H11A* 3'UTRs was sufficient to accelerate melanoma development using our embryonic stem cell-genetically engineered mouse model (ESC-GEMM) platform (Bok et al., 2019). 1q^{AMP} ceRNA constructs were generated in which the *CEP170*, *NUCKS1*, or *ZC3H11A* 3'UTRs were linked to the GFP cDNA and expressed under the control of the Dox-inducible TRE promoter (referred to as TRE-CEP170, TRE-NUCKS1, and TRE-ZC3H11A). TRE-GFP lacking a 3'UTR was used as control. These constructs were targeted by recombination-

mediated cassette exchange to the homing cassette in BP (LSL-Braf^{V600E}; Pten$^{FL/WT}$) embryonic stem cells (ESCs) (Bok et al., 2019). These ESCs also harbor Tyr-CreERt2 and CAGs-LSL-rtTA3 alleles for melanocyte-specific driver allele recombination and activation of the Dox-inducible transgenes, respectively (**Figure S3G**). Chimeras were generated with targeted BP ESCs. At 3-4 weeks of age, chimeras were topically treated with 4-hydroxytamoxifen (4OHT) on their back skin to induce Cre activity and then immediately placed on a Dox-containing diet to induce 3'UTR expression. TRE-CEP170 chimeras, but not TRE-NUCKS1 and TRE-ZC3H11A chimeras, exhibited accelerated melanoma formation, reducing tumor-free and overall survival (**Figure 3D and 3E**). The rapid tumor growth in the BP model precludes significant development of metastatic disease. Accordingly, we did not observe macroscopic metastases in any of the genotypes except for a single lung metastasis in a TRE-CEP170 chimera (not shown). Thus, to assess if the 1q^{AMP} ceRNAs also augmented aggressive phenotypes of mouse melanoma cells, we established primary melanoma cell lines from TRE-CEP170 (BPC), TRE-NUCKS1 (BPN), TRE-ZC3H11A (BPZ) and TRE-GFP (BPG) chimeras. BPC cells were significantly more invasive than BPG cells, while BPN and BPZ were moderately more invasive (**Figure 3F**). Thus, the 1q^{AMP} ceRNAs *CEP170*, *NUCKS1*, *ZC3H11A* promote melanoma progression and metastasis.

1q^{AMP} ceRNAs sequester tumor suppressive miRNAs

To define the mechanism underlying the oncogenic effect of the 1q^{AMP} ceRNAs, we assessed the ability of the *CEP170*, *NUCKS1*, and *ZC3H11A* 3'UTRs to function as miRNA sponges. To this end we created a series of luciferase reporters harboring binding sites for the miRNAs predicted to engage in the 1q^{AMP} ceRNA network (**Table S5**). Luc-MRE reporters were expressed in WM793 and A375 melanoma cells with our without the *CEP170*, *NUCKS1*, or *ZC3H11A* 3'UTRs (**Figure S4A**). This identified miRNAs that are expressed and active (i.e., Luc-MRE reporter activity is reduced compared to empty Luc control reporter) as well as those

that are sequestered by the 1q^{AMP} ceRNAs (i.e., Luc-MRE reporter activity is increased by the *CEP170*, *NUCKS1*, or *ZC3H11A* 3'UTRs compared to GFP). This analysis revealed that: (i) miR-135, miR-141, miR-144, miR-200a, and miR-203 are sponged by the *CEP170* 3'UTR: (ii) miR-135, miR-137, and miR-203 are sponged by the *NUCKS1* 3'UTR; and (iii) miR-101, miR-125, miR-137, miR-144, miR-200bc, and miR-497 are sponged by the *ZC3H11A* 3'UTR (**Figures 4A-C and S4B-D**). Of note, miR-135, miR-137, miR-144, and miR-203 are sequestered by two 3'UTRs, and the combined expression of the 1q^{AMP} ceRNA 3'UTRs further enhanced Luciferase activity of these four Luc-MRE reporters (**Figure 4D**).

To test direct interaction of these 9 miRNAs with the 1q^{AMP} ceRNAs, we performed RNA pulldowns using biotinylated probes targeting the GFP sequence in WM793 melanoma cells expressing the *CEP170*, *NUCKS1*, or *ZC3H11A* 3'UTRs (**Figure S4E**). These analyses revealed that: (i) miR-135, miR-141, miR-144, miR-200a, and miR-203 bound the *CEP170* 3'UTR; (ii) miR-135, miR-137, and miR-203 bound the *NUCKS1* 3'UTR; and (iii) miR-101, miR-125, miR-137, miR-144, miR-200bc, and miR-497 bound the *ZC3H11A* 3'UTR (**Figure 4E**). Finally, to further validate the interaction of the 1q^{AMP} ceRNAs with these miRNAs, we transfected miRNA mimics into WM793 melanoma cells. As expected, mimics of: (i) miR-135, miR-141, miR-144, miR-200a, and miR-203 decreased *CEP170* expression; (ii) miR-135, miR-137, and miR-203 mimics decreased *NUCKS1* expression; and (iii) miR-101, miR-125, miR-137, miR-144, miR-200bc, and miR-497 mimics reduced *ZC3H11A* expression (**Figure 4F**). Thus, the *CEP170*, *NUCKS1*, and *ZC3H11A* 3'UTRs directly bind to and selectively impair the activity of 9 miRNAs.

To assess the stoichiometry of 1q^{AMP} ceRNAs and the 9 interacting miRNAs, we determined the absolute copy numbers of the endogenous transcripts in A375 and WM793 melanoma cells by Droplet Digital PCR. Notably, with one exception (miR-125) the *CEP170*, *NUCKS1*, and *ZC3H11A* mRNAs are equal to or are more abundant than these target miRNAs (**Figure S4F and S4G**). Moreover, with the exception of miR-125, the number of MREs in the

$1q^{AMP}$ ceRNAs significantly exceeded the number of molecules of their corresponding miRNAs (**Figure 4G**), suggesting that in $1q^{AMP}$ melanoma abundant *CEP170*, *NUCKS1*, and *ZC3H11A* mRNAs can competitively sequester miRNAs.

If overexpression of the $1q^{AMP}$ ceRNAs reduces the activity of the bound miRNAs toward other targets, these miRNAs may have tumor suppressive potential. To test this, we delivered miRNA mimics and inhibitors to WM793 and 1205Lu melanoma cells and assessed the effects on cell invasion. Notably, 8 out of 9 miRNA mimics reduced cell invasion, and 5 (WM793) and 7 (1205Lu) miRNA inhibitors increased cell invasion to varying extents (**Figures 4G, 4I, and S4H**). Finally, the expression of miR-141, miR-200a/b/c, and miR-203a is reduced in metastatic melanoma compared to primary tumors in TCGA skin cutaneous melanoma dataset, also supporting tumor suppressor roles for these miRNAs (**Figure S4I**). Thus, $1q^{AMP}$ ceRNAs bind to and inhibit miRNAs having tumor suppressor potential in melanoma.

$1q^{AMP}$ ceRNAs promote melanoma metastasis in a miRNA-dependent manner

To test if the oncogenic potential of the $1q^{AMP}$ ceRNAs is dependent on the interaction with miRNAs, we silenced *Dicer* in WM793 melanoma cells to acutely inhibit global miRNA biogenesis (**Figure S5A**). Silencing of *Dicer* abolished the pro-invasion effects of individual and combined $1q^{AMP}$ ceRNA overexpression (**Figure 5A**). To verify this was through sequestering the identified tumor suppressor miRNAs, the relevant MREs in the *CEP170*, *NUCKS1*, and *ZC3H11A* 3'UTR overexpression constructs were mutated to prevent miRNA binding to 3'UTRs. Specifically, we mutated: (i) the miR-135, miR-141/200a, miR-144, and miR-203 MREs in *CEP170*; (ii) the miR-135, miR-137, and miR-203 MREs in *NUCKS1*; and (iii) the miR-101/144, miR-137, miR-200bc, and miR-497 MREs in *ZC3H11A*. While overexpression of the wildtype *CEP170*, *NUCKS1*, and *ZC3H11A* 3'UTRs increased the invasion of WM793 and A375 melanoma cells, the MRE-mutant 3'UTRs had no effect (**Figures 5B-D and S5B-D**). Furthermore, the wildtype 3'UTRs but not the MRE-mutant 3'UTRs rescued cell invasion in

melanoma cells transfected with the corresponding miRNA mimics (**Figures 5B-D and S5B-D**). Finally, expression of wildtype but not MRE-mutant *CEP170*, *NUCKS1*, or *ZC3H11A* 3'UTR constructs in 1205Lu cells in which the corresponding endogenous $1q^{AMP}$ ceRNAs were silenced rescued cell invasion in vitro (**Figure S5E**) and lung metastasis following intravenous transplantation in NSG mice (**Figure 5F**). Thus, the pro-metastatic potential of the $1q^{AMP}$ ceRNAs depends on their ability to sequester their respective tumor suppressor miRNA targets.

The contribution of miR-101, miR-135, miR-137, miR-141, miR-144, miR-200, miR-203, and miR-497 to the oncogenic effects of endogenously expressed $1q^{AMP}$ ceRNAs was further tested using miRNA inhibitors and Target Site Blockers (TSBs). Knockdown of *CEP170*, *NUCKS1*, or *ZC3H11A* in 1205Lu melanoma cells reduced the activity of the respective Luc-MRE reporters (**Figure S5F-H**), indicating that silencing of $1q^{AMP}$ ceRNAs enhances activity of their miRNA targets. Indeed, co-transfection of the corresponding miRNA inhibitors (i.e., [i] miR-135, miR-141, miR-144, miR-200a, or miR-203 inhibitors in *CEP170*-silenced cells; [ii] miR-135, miR-137, or miR-203 inhibitors in *NUCKS1*-silenced cells; and [iii] miR-101, miR-137, miR-144, miR-200bc, or miR-497 inhibitors in *ZC3H11A*-silenced cells) rescued the repression of the Luc-MRE reporters (**Figure S5F-H**). Similarly, the decrease in cell invasion upon $1q^{AMP}$ ceRNA silencing was partially rescued by the respective miRNA inhibitors (**Figure 5G-H**).

TSBs block endogenous ceRNA-miRNA interactions and thereby reduce ceRNA-mediated miRNA sequestration. Delivery of TSBs to 1205Lu melanoma cells targeting the respective MREs on *CEP170*, *NUCKS1*, or *ZC3H11A* affirmed the miRNA sponge effects of endogenous $1q^{AMP}$ ceRNAs, where the individual TSBs inhibited invasion of 1205Lu melanoma cells (**Figure 5J**). To test the effect of blocking the binding of all relevant miRNAs to *CEP170*, *NUCKS1*, or *ZC3H11A*, we delivered combinations of TSBs to 1205Lu cells. Phenocopying the effects of $1q^{AMP}$ ceRNA silencing, TSBs significantly reduced the invasion of 1205Lu cells in transwell assays (**Figure 5K**) and the seeding to the lungs upon intravenous transplantation into NSG

mice (**Figure 5L**). Thus, $1q^{AMP}$ ceRNAs promote melanoma progression and lung metastasis by sequestering 8 tumor suppressive miRNAs.

$1q^{AMP}$ ceRNAs de-repress pro-metastatic genes by sequestering shared miRNAs.

A thorough literature search identified 301 metastasis-related genes that are validated targets of the 8 tumor suppressor miRNAs sequestered by the $1q^{AMP}$ ceRNAs (**Figure S6A; Table S6**). Among these are 75 genes whose expression significantly correlates (FDR $p<0.0001$, Spearman ≥ 0.25) with expression of $1q^{AMP}$ ceRNAs in the TCGA SKCM dataset (**Figure S6B**). Moreover, 49 out of these 75 putative effectors are significantly overexpressed in melanoma metastases compared to primary tumors (**Figure S6C**) and 24 of these are shared putative effectors of two or all three $1q^{AMP}$ ceRNAs (**Figure S6D**). qRT-PCR revealed that $1q^{AMP}$ ceRNA overexpression in melanoma cell lines increased the mRNA levels of 7 of these putative ceRNA effectors (data not shown), and immunoblot analyses revealed increases in the expression of all 7 (ZEB1, ZEB2, ROCK1, ROCK2, SP1, SUZ12, and BMI1) in WM793 melanoma cells engineered to overexpress the 3'UTRs of *CEP170*, *NUCKS1*, and *ZC3H11* (**Figures 6A and S6E**). Finally, the expression of these putative effectors was suppressed upon silencing of endogenous *CEP170*, *NUCKS1*, and *ZC3H11A* in 1205Lu melanoma cells and their levels were rescued when the expression of the *CEP170*, *NUCKS1*, or *ZC3H11A* 3'UTRs were rescued (**Figure 6B**).

Notably, the regulation of these putative effectors by $1q^{AMP}$ ceRNAs was miRNA-dependent. First, transfection of WM793 melanoma cells with respective miRNA mimics suppressed the expression of the 7 putative effectors (**Figure 6C**). Second, concomitant overexpression of the *CEP170*, *NUCK1*, or *ZC3H11A* 3'UTRs limited the repression of these effectors by the miRNA mimics (**Figure 6C**). Third, transfection of 1205Lu melanoma cells with miRNA inhibitors negated effects of silencing endogenous *CEP170*, *NUCK1*, or *ZC3H11A* on the expression of these seven effectors (**Figure 6D**). Finally, blocking MREs of endogenous *CEP170*, *NUCK1*, or

ZC3H11A mRNAs using TSBs reduced expression of these effectors (**Figures 7E and S6F**). Thus, *CEP170*, *NUCKS1*, and *ZC3H11A* function as ceRNAs that control expression of the pro-metastatic genes *ZEB1*, *ZEB2*, *ROCK1*, *ROCK2*, *SP1*, *SUZ12*, and *BMI1* by sequestering shared miRNAs.

Evidence for the 1q^{AMP} ceRNA network in multiple cancer types

Chromosome 1q copy number alterations occur in multiple other cancer types. To investigate the contribution of the 1q^{AMP} ceRNA network to tumor progression and metastasis across cancer types we queried TCGA for concomitant copy number alterations of *CEP170*, *NUCKS1*, and *ZC3H11A*. Significant co-amplifications and co-gains of *CEP170*, *NUCKS1*, and *ZC3H11A* were identified in breast cancer, colon adenocarcinoma, hepatocellular carcinoma, lung adenocarcinoma and lung squamous cell carcinoma (**Figure 7A**). Notably, the expression of *CEP170*, *NUCKS1*, and *ZC3H11A* strongly correlates with the expression of *ZEB1*, *ZEB2*, *ROCK1*, *ROCK2*, *SP1*, *SUZ12*, and *BMI1* (**Figure 7B**), suggesting the 1q^{AMP} ceRNA network is also functional in these cancer types. Interestingly, a positive correlation between 1q^{AMP} ceRNAs and the pro-metastatic effectors *ZEB1*, *ZEB2*, *ROCK1*, *ROCK2*, *SP1*, *SUZ12*, and *BMI1* was also evident in some cancers lacking significant alterations of chromosome 1q copy number, including prostate adenocarcinoma, stomach adenocarcinoma, and uveal melanoma (**Figure 7B**). These findings suggest that a ceRNA network directed by the chromosome 1q *CEP170*, *NUCKS1*, and *ZC3H11A* ceRNAs contributes to the formation and/or progression of several cancer types.

DISCUSSION

The studies reported herein establish that the chromosome 1q amplification activates a novel oncogenic ceRNA network that promotes tumor progression and metastasis of melanoma and

potentially other tumor types. Specifically, this complex $1q^{AMP}$ ceRNA network is controlled by three mRNAs, *CEP170*, *NUCKS1*, and *ZC3H11A* that sequester 8 tumor suppressive miRNAs, impairing their repressive activity towards genes that have established roles in driving metastasis.

The notion that ceRNAs sequester select miRNAs to post-transcriptionally control gene expression prompted several mathematical modeling studies seeking to understand ceRNA circuits (Ala et al., 2013; Bosia et al., 2013; Chiu et al., 2018; Figliuzzi et al., 2013; Hausser and Zavolan, 2014; Jens and Rajewsky, 2014; Sumazin et al., 2011). These models differed in their presumed conditions of miRNA action and competition, and this resulted in various predictions of optimal miRNA:target ratios that are necessary for efficient ceRNA function and crosstalk. Further, quantitative miRNA and target copy number measurements combined with reporter assays led to the proposal of two conflicting models of miRNA binding: the hierarchical and non-hierarchical models (Bosson et al., 2014; Denzler et al., 2014, 2016). Both models predict a ceRNA must add a relatively large number of MREs to a network to elicit biologically meaningful changes in expression, and this MRE number is much greater in the non-hierarchical model (Bosson et al., 2014; Denzler et al., 2014, 2016). Indeed, while the hierarchical model concludes that ceRNA crosstalk is possible under certain conditions, the non-hierarchical model argues against ceRNA crosstalk being physiologically relevant. This is in stark contrast to the extensive experimental evidence supporting ceRNA functions of mammalian mRNAs (Chiu et al., 2017; Gao et al., 2016; Gilot et al., 2017; Jeyapalan et al., 2011; Karreth et al., 2011; Powers et al., 2016; Rutnam and Yang, 2012; Sumazin et al., 2011; Tay et al., 2011). Contributing to this controversy, many conditions that likely affect ceRNA potential, reviewed by Ponting and colleagues (Smillie et al., 2018), were not considered in the modeling- and reporter-based studies. On the other hand, several studies supporting ceRNA functions do not unequivocally demonstrate that crosstalk identified was miRNA-dependent. Indeed, while sharing MREs with other transcripts is the defining feature of a ceRNA, it is a poor predictor of ceRNA activity, and

it is not clear if a generalizable model can be devised that accurately predict the identity of ceRNA/effector pairs and the extent of crosstalk. Thus, as shown here for the $1q^{AMP}$ ceRNAs present in melanoma, ceRNAs predictions have to be based on shared MREs and supported by positive expression correlations, followed by rigorous experimental validation.

Compared to our previous studies where ceRNA predictions were based solely on shared MREs (Karreth et al., 2011; Tay et al., 2011), here we assumed that elevated expression of pathophysiological $1q^{AMP}$ ceRNAs with high basal levels would provide sufficient MREs to provoke biologically meaningful expression changes of their effectors. Further, we incorporated expression analyses to identify ceRNA/effector pairs that have a positive correlation and that share MREs. The resulting ceRNA network was highly interconnected, with numerous effectors predicted to be regulated by more than one ceRNA. Notably, a subnetwork emerged consisting of several putative ceRNAs localized on chromosome 1q, including *CEP170*, *NUCKS1*, and *ZC3H11A*, which has numerous overlapping effectors, i.e., transcripts that can be regulated by more than one $1q^{AMP}$-localized ceRNA. The concomitant overexpression of *CEP170*, *NUCKS1*, and *ZC3H11A* upon chromosome 1q copy number gain has two intriguing consequences. First, as *CEP170*, *NUCKS1*, and *ZC3H11A* share MREs for the same miRNA families, their overexpression sequesters more copies of these miRNAs. Second, two different ceRNAs can regulate the same effector through different sets of miRNAs. Overall, this raises the ceRNA:miRNA ratio to augment miRNA sequestration. As the robustness of ceRNA crosstalk increases with the number of sequestered miRNAs (Ala et al., 2013; Chiu et al., 2018), concomitant overexpression of $1q^{AMP}$ ceRNAs also augments expression of effectors normally suppressed by these miRNAs. Consistent with this notion, combined overexpression of the *CEP170*, *NUCKS1*, and *ZC3H11A* 3'UTRs promotes migration and invasion more potently that overexpression of individual $1q^{AMP}$ ceRNAs. These findings support the hypothesis that the concerted deregulation of multiple ceRNAs will provoke more robust effects (Smillie et al., 2018).

miRNA sequestration is unlikely to have significant effects on gene expression regulation under homeostatic conditions, for instance in response to physiological oscillation of ceRNA gene transcription. Rather, miRNA sequestration by ceRNAs may be critical during acute stimuli that elicit significant but short-lived expression changes (e.g., stress responses) or when cells transition to new physiological (e.g., differentiation) or pathological (e.g., cell transformation) states associated with distinct gene expression programs. Further, ceRNAs can be classified as exclusive ceRNAs and network ceRNAs based on their mode of action. Exclusive ceRNAs are individual transcripts that sequester a single miRNA family, and unusual circumstances may be required for their activity. For instance, amplification of *MYCN* in neuroblastoma leads to >100-fold overexpression, providing almost 20% of the let-7 target site pool, and a MRE:miRNA ratio ranging from of 3.7 to >10 (Powers et al., 2016). Another example of an exclusive ceRNA is *TYRP1* that sequesters miR-16 in melanoma through three non-canonical target sites that do not support *TYRP1* mRNA decay (Gilot et al., 2017). By contrast, network ceRNAs, as highlighted by $1q^{AMP}$ ceRNAs, sequester multiple miRNAs that can converge on the regulation of a biological process such as metastasis, as demonstrated herein. Effective miRNA sequestration can be mediated by the presence of multiple MREs and atypical expression changes or non-canonical MREs are not strictly required. Indeed, the $1q^{AMP}$ ceRNAs harbor canonical 8mer and 7mer MREs for the relevant miRNAs and their expression, while more abundant than that of the sequestered miRNAs, does not reach levels observed for *MYCN*. Neither *MYCN* and *TYRP1* (Gilot et al., 2017; Powers et al., 2016) nor the $1q^{AMP}$ ceRNAs (data not shown) reduce miRNA levels, indicating that, given the absence of extensive target site complementarity, target RNA-directed miRNA degradation (TDMD) plays no part in the mechanism of action of these exclusive and network ceRNAs.

Many studies portray ceRNAs as players in linear axes where they sequester a single miRNA to regulate a single effector. However, given that miRNAs repress numerous targets, it is conceivable that both exclusive and network ceRNAs prompt phenotypes by regulating a pool

of effectors. Using several orthogonal approaches, we unequivocally demonstrate that sequestration of 8 miRNAs underlies the oncogenic effects of the $1q^{AMP}$ ceRNAs. These miRNAs possess tumor suppressive activity, including in melanoma, and their combined sequestration perturbs expression of multiple target mRNAs. Indeed, our focused search for pro-metastatic effectors identified dozens of candidates, seven of which (ZEB1, ZEB2, ROCK1, ROCK2, SP1, SUZ12, and BMI1) were validated to be regulated by the $1q^{AMP}$ ceRNAs in a miRNA-dependent manner. We note that it is likely that additional effectors are regulated by the $1q^{AMP}$ ceRNAs, which could further contribute to melanoma progression and metastasis. In addition, it remains unknown whether there are a few key effectors of the $1q^{AMP}$ ceRNAs or whether an expansive effector program acts in concert to mediate $1q^{AMP}$ ceRNA-driven progression and metastasis. While the latter scenario appears more likely given the moderate expression changes of the investigated effectors, their interplay and relative contribution to the phenotype may be context-dependent. For instance, ZEB1 and ZEB2 are involved in melanoma phenotype-switching, where ZEB2 promotes proliferation of primary tumors and metastatic lesions and ZEB1 stimulates melanoma invasion (Caramel et al., 2013; Denecker et al., 2014; Vandamme et al., 2020). $1q^{AMP}$ ceRNAs may therefore promote metastatic dissemination by enhancing expression of either ZEB2 or ZEB1 at different stages of this process. Because the posttranscriptional regulation of ZEB2 and ZEB1 by $1q^{AMP}$ ceRNAs occurs in addition to their transcriptional control, ZEB2 and ZEB1 expression could be increased without perturbing the relative ZEB2:ZEB1 ratio. Numerous studies also implicate ROCK1, ROCK2, SP1, SUZ12, and BMI1 in melanoma and/or the metastasis of other cancer types, supporting the notion that the $1q^{AMP}$ ceRNAs elicit their effects by controlling a complex miRNA/effector network. Moreover, *CEP170*, *NUCKS1*, and *ZC3H11A* expression is positively correlated with their effectors in several additional cancer types, highlighting a broad tumorigenic function of the $1q^{AMP}$ ceRNA network.

In summary, we have systematically identified a complex pro-metastatic ceRNA network directly from patient level genomics data and highlight a key regulatory mechanism controlled by three genes, *CEP170*, *NUCKS1*, and *ZC3H11A*, that are concomitantly subjected to copy number alterations. Our study highlights how ceRNA cooperation can strongly distort regulatory networks to drive cancer progression, which we posit is a major mechanism underlying the oncogenic effects of copy number alterations. ceRNA networks should therefore be considered in future studies of copy number alterations, especially when amplifications or deletions lack obvious protein-coding driver genes.

ACKNOWLEDGMENTS

We are grateful for Karreth lab members for helpful discussions, and to J. Cleveland and Y. Tay for critical reading of the manuscript. We are grateful to A. Angarita for help with molecular cloning. This work was supported by grants from the National Institutes of Health (R03CA227349, R01CA259046) and from the Melanoma Research Alliance (https://doi.org/10.48050/pc.gr.75702) to F.A.K. This work was also supported by the Gene Targeting Core, which is funded in part by Moffitt's Cancer Center Support Grant (P30CA076292).

AUTHOR CONTRIBUTIONS

F.A.K conceived and supervised the project. X.X. designed and performed the majority of experiments. K.W. identified validated miRNA targets and O.V. assisted with cell line derivation. A.V., O.E., and X.Y. performed ceRNA network predictions. X.X. and F.A.K. wrote the manuscript with input from all authors.

DECLARATION OF INTERESTS

The authors declare no competing interests

FIGURE LEGENDS

Figure 1. Amplification and overexpression of predicted 1q ceRNA genes is associated with melanoma metastasis

(A) The metastatic melanoma ceRNA network. Central triangles represent amplified ceRNA genes and peripheral circles represent putative effectors.

(B) The number of putative effectors for each ceRNA gene.

(C) Copy number alterations of *CEP170*, *NUCKS1*, and *ZC3H11A* in TCGA cutaneous melanoma samples. *CEP170* and *ZC3H11A* are gained/amplified in 203 out of 367 samples, while *NUCKS1* is gained/amplified in 200 samples. All three genes are co-gained/amplified in 191 samples.

(D) Correlation of *CEP170*, *NUCKS1*, and *ZC3H11A* expression in TCGA cutaneous melanoma samples.

(E) Expression of *CEP170*, *NUCKS1*, and *ZC3H11A* in primary and metastatic cutaneous melanoma samples from TCGA. Mean ± SEM is shown; ** $p < 0.01$, *** $p < 0.001$.

(F) GSEA analysis of TCGA cutaneous melanoma samples associates *CEP170*, *NUCKS1*, and *ZC3H11A* expression with a melanoma metastasis gene signature.

See also Figure S1.

Figure 2. $1q^{AMP}$ ceRNAs have oncogenic effects in melanoma cells in vitro

(A) Anchorage-independent growth of A375 and WM793 cells expressing GFP, GFP-CEP170-3'UTR, GFP-NUCKS1-3'UTR, GFP-ZC3H11A-3'UTR, or the combination of the three 3'UTRs (Combo). Representative images are show on the left, quantifications are shown on the right.

(B) Quantification of migrated cells in transwell migration assays using the cell lines shown in (A). (C) Quantification of invasive cells in transwell invasion assays using the cell lines shown in (A). (D) Anchorage-independent growth of 1205Lu cells expressing shRNAs targeting *CEP170*, *NUCKS1*, or *ZC3H11A*. A scrambled shRNA was used as negative control. Representative images are show on the left, quantifications are shown on the right.

(E) Quantification of migrated cells in transwell migration assays using the cell lines shown in (D). (F) Quantification of invasive cells in transwell invasion assays using the cell lines shown in (D).

N = 3 biological replicates; two-sided t test. Values represent mean ± SEM; * $p < 0.05$, ** $p < 0.01$, *** $p < 0.001$. See also Figure S2.

Figure 3. 1q^{AMP} ceRNAs enhance melanoma metastasis in vivo

(A-B) Luciferase tagged A375 (A) and WM793 (B) cells expressing GFP, GFP-CEP170-3'UTR, GFP-NUCKS1-3'UTR, GFP-ZC3H11A-3'UTR, or the combination of the three 3'UTRs (Combo) were injected into NSG mice subcutaneously (A375) or intravenously (WM793). Quantification of the luminescence signals in lungs after 28 days (A375) or 60 days (WM793) is shown.

(C) Luciferase tagged 1205Lu cells expressing shRNAs against *CEP170*, *NUCKS1*, or *ZC3H11A* or a scrambled control were intravenously injected into NSG mice and the luminescence signal in lungs was quantified after 25 days.

(D-E) Overall survival (D) and tumor-free survival (E) of BP chimeras expressing GFP, GFP-CEP170-3'UTR, GFP-NUCKS1-3'UTR, or GFP-ZC3H11A-3'UTR in melanocytes.

(F) Quantification of transwell invasion of primary melanoma cells derived from GFP, GFP-CEP170-3'UTR, GFP-NUCKS1-3'UTR, or GFP-ZC3H11A-3'UTR chimeras.

Each data point in (A-C) represents one mouse. Values represent mean ± SEM. * $p < 0.05$, ** $p < 0.01$, *** $p < 0.001$. See also Figure S3.

Figure 4. 1q^{AMP} ceRNAs sequester tumor suppressor miRNAs

(A) Luciferase assays using dual luciferase reporters harboring MREs for miR-135-5p, miR-141-3p, miR-144-3p, miR-200-3p, or miR-203-3p in WM793 cells expressing GFP or GFP-CEP170-3'UTR. Luciferase activity was normalized to the reporter without MRE (vector).

(B) Luciferase assays using dual luciferase reporters harboring MREs for miR-135-5p, miR-137, or miR-203-3p in WM793 cells expressing GFP or GFP-NUCKS1-3'UTR. Luciferase activity was normalized to the reporter without MRE (vector).

(C) Luciferase assays using dual luciferase reporters harboring MREs for miR-101-3p, miR-125-5p, miR-137, miR-144-3p, miR-200-3p, or miR-497-5p in WM793 cells expressing GFP or GFP-ZC3H11A-3'UTR. Luciferase activity was normalized to the reporter without MRE (vector).

In (A-C), asterisks (*, **) indicate comparison of Luc-MRE reporter vs. empty control Luc reporter (Vector) and pound symbols ($^{\#}$, $^{\#\#}$) indicate comparison of 3'UTR vs. GFP.

(D) Luciferase assays using dual luciferase reporters harboring MREs for miR-135-5p, miR-137, miR-144-3p, or miR-200-3p in WM793 cells expressing the $1q^{AMP}$ ceRNA 3'UTRs individually or in combination. Luciferase activity was normalized to the reporter without MRE (vector), not shown.

(E) RNA pulldown of GFP, GFP-CEP170-3'UTR, GFP-NUCKS1-3'UTR, or GFP-ZC3H11A-3'UTR followed by qRT-PCR for the indicated miRNAs shows the relative enrichment of bound miRNAs. (F) qRT-PCR showing the relative expression of endogenous *CEP170*, *NUCKS1*, and *ZC3H11A* in 1205Lu cells upon transfection of the indicated miRNA mimics.

(G) Copy number of the indicated mature miRNAs and the corresponding MREs present in endogenous *CEP170*, *NUCKS1*, *ZC3H11A* in A375 and WM793 cells were quantified by Droplet Digital PCR.

(H) Quantification of invasive WM793 cells in transwell invasion assays upon transfection with the indicated miRNA mimics.

(I) Quantification of invasive WM793 cells in transwell invasion assays upon transfection with the indicated miRNA inhibitors.

N = 3 biological replicates; two-sided t test. Values represent mean ± SEM. * $p < 0.05$, ** $p < 0.01$, *** $p < 0.001$, $^{\#}$ $p < 0.05$, $^{\#\#}$ $p < 0.01$. See also Figure S4.

Figure 5. $1q^{AMP}$ ceRNAs-directed melanoma cell invasion and metastasis is miRNA dependent

(A) Quantification of transwell invasion of WM793 cells overexpressing GFP (gray bars) or the GFP-linked $1q^{AMP}$ ceRNA 3'UTRs individually or in combination. WM793 cells were transfected with and siRNA pool targeting Dicer or a non-targeting control siRNA pool. Asterisks indicate comparisons of 3'UTR overexpression (light/dark blue bars) vs. control (gray bars) and pound

symbol indicates comparison of si-Dicer vs. non-targeting siRNA in vector control samples (gray bars).

(B-D) Quantification of transwell invasion of WM793 cells upon transfection with the indicated miRNA mimics. WM793 cells overexpress GFP, or wildtype or MRE-mutant GFP-CEP170-3'UTR (B), GFP-NUCKS1-3'UTR (C), or GFP-ZC3H11A-3'UTR (D). Asterisks indicate comparisons of GFP vs. 3'UTR-WT vs. 3'UTR-Mut and pound symbols indicate comparisons of miRNA mimics vs. scrambled control in GFP control samples (blue bars).

(E) Quantification of transwell invasion of 1205Lu cells in which the 1qAMP ceRNAs were knocked-down followed by restoration with either wildtype or MRE-mutant GFP-CEP170-3'UTR, GFP-NUCKS1-3'UTR, or GFP-ZC3H11A-3'UTR.

(F) Luciferase-labeled 1205Lu cells from (E) were intravenously injected into NSG mice and the luminescence signal in lungs was quantified after 25 days. In (E-F), asterisks indicate comparisons of control vs. 3'UTR-WT vs. 3'UTR-Mut and pound symbols indicate comparisons of ceRNA shRNAs (dark blue bars) vs. control shRNA (gray bar).

(G-I) Quantification of transwell invasion of CEP170- (G), NUCKS1- (H), or ZC3H11A-silenced (I) 1205Lu cells upon transfection with the indicated miRNA inhibitors. Asterisks indicate comparisons of ceRNA shRNA + miRNA inhibitor (light blue bars) vs. ceRNA shRNA (dark blue bars) and pound symbols indicate comparisons of ceRNA shRNAs (dark blue bars) vs. control shRNA (gray bars).

(J) Quantification of transwell invasion of 1205Lu cells transfected with the indicated target site blockers (TSBs). Asterisks indicate comparisons of TSBs (light blue bars) vs. control TSB (gray bars).

(K) Quantification of transwell invasion of 1205Lu cells transfected with TSB combinations to block all relevant MREs on endogenous *CEP170*, *NUCKS1*, or *ZC3H11A*. Asterisks indicate comparisons of TSBs (light blue bars) vs. control TSB (gray bars).

(L) Luciferase-labeled 1205Lu cells were transfected with TSB combinations to block MREs on endogenous *CEP170*, *NUCKS1*, or *ZC3H11A* followed by intravenous injection into NSG mice. Quantification of the luminescence signal in lungs after 25 days is shown. Asterisks indicate comparisons of TSBs (light blue) vs. control TSB (gray).

N = 3 biological replicates; two-sided t test. Values represent mean ± SEM. * $p < 0.05$, ** $p < 0.01$, *** $p < 0.001$, $^{\#}$ $p < 0.05$, $^{\#\#}$ $p < 0.01$, $^{\#\#\#}$ $p < 0.001$, ns not significant. See also Figure S5.

Figure 6. 1q^{AMP} ceRNAs de-repress pro-metastatic genes by sequestering shared miRNAs.

(A) Western blot of effector levels upon expression of GFP-CEP170-3'UTR, GFP-NUCKS1-3'UTR, or GFP-ZC3H11A-3'UTR in WM793 cells.

(B) Western blot of effector levels upon 1q^{AMP} ceRNA silencing in WM793 cells and restoration with GFP-CEP170-3'UTR, GFP-NUCKS1-3'UTR, or GFP-ZC3H11A-3'UTR.

(C) Heatmap showing expression changes of the 1q^{AMP} ceRNA effectors detected by qRT-PCR. The indicated miRNA mimics were transfected into WM793 cells expressing GFP control, GFP-CEP170-3'UTR, GFP-NUCKS1-3'UTR, or GFP-ZC3H11A-3'UTR. Color bar represents Log_2 fold change of expression. Log_2 fold change values and p-values represented in the heatmap are listed in Table S7

(D) Heatmap showing expression changes of the 1q^{AMP} ceRNA effectors detected by qRT-PCR. The indicated miRNA inhibitors were transfected into 1205Lu cells in which endogenous *CEP170*, *NUCKS1*, or *ZC3H11A* are knocked down. Color bar represents Log_2 fold change of expression. Log_2 fold change values and p-values represented in the heatmap are listed in Table S8

(E) Western blot of effector levels in1205Lu cells transfected with TSBs combinations to block the relevant MREs on endogenous *CEP170*, *NUCKS1*, or *ZC3H11A*.

N = 3 biological replicates. See also Figure S6.

Figure 7. Evidence for the 1q^{AMP} ceRNA network in multiple cancer types

(A) Venn diagrams showing co-amplifications and co-gains of *CEP170*, *NUCKS1*, *ZC3H11A* in breast cancer (BRCA), colon adenocarcinoma (COAD), hepatocellular carcinoma (HCC), lung adenocarcinoma (LUAD), and lung squamous carcinoma (LUSC) in TCGA datasets.

(B) Heatmaps showing the correlation between 1q^{AMP} ceRNAs and effectors in breast cancer (BRCA), colon adenocarcinoma (COAD), hepatocellular carcinoma (HCC), lung adenocarcinoma (LUAD), and lung squamous carcinoma (LUSC), stomach adenocarcinoma (STAD) and uveal melanoma (UVM). Spearman correlation values and p-values represented in the heatmap are listed in Table S9

Methods

RESOURCE AVAILABILITY

Lead contact

Further information and requests for resources and reagents should be directed to and will be fulfilled by the lead contact, Florian A. Karreth (florian.karreth@moffitt.org).

Materials availability

Plasmids will be deposited at Addgene. Targeted ES cell lines/mouse strains are available upon request from the lead contact.

Data and code availability

- All data reported in this paper will be shared by the lead contact upon request.
- This paper does not report original code.
- Any additional information required to reanalyze the data reported in this paper is available from the lead contact upon request

EXPERIMENTAL MODEL AND SUBJECT DETAILS

Cell lines and culture conditions

Human melanoma cell lines WM793 and 1205Lu were provided by M. Herlyn (Wistar). A375 were obtained from ATCC, HEK293T Lenti-X cells were purchased from Takara. Primary mouse melanoma cell lines were isolated from mouse melanomas. Briefly, tumors were washed in 70% ethanol and washed in PBS, chopped into small pieces and dissociated using the Milteny Tumor Dissociation Kit (Milteny, #130-095-929) following the manufacturer's recommendations. Digested tissues were filtered using MACS® SmartStrainers (70 µm) (Milteny, #130-098-462)

into a conical tube with 5ml of RPMI-1640 containing 5% FBS and 1% Pen/Strep to obtain a single cell suspension. Cells were collected by centrifugation, resuspended in 10 ml of RPMI-1640 containing 5% FBS and 1% Pen/Strep, and plated in a 10cm dish. After 1-2 passage, cells were transplanted subcutaneously into the flanks of NSG mice for in vivo passaging. Subcutaneous tumors from NSG mice were processed as above and used to establish the murine cell lines. All cell lines were cultured in a humidified atmosphere at 37°C and 5% CO_2. Melanoma cell lines were cultured in RPMI-1640 (Lonza) containing 5% FBS (Sigma). HEK293T Lenti-X were cultured in DMEM (VWR) containing 10% FBS. All cell lines were confirmed to be mycoplasma-free by the MycoAlert Mycoplasma Detection Kits (Lonza).

Animal models

All animal experiments were conducted in accordance with an IACUC protocol approved by the University of South Florida. NSG mice were obtained from JAX (Stock No: 005557) and bred in-house. 6-week-old male and female NSG mice were randomly divided into groups (at least 5 mice per group). $1.5x10^5$ 1205Lu or $5x10^5$ WM793 melanoma cells, were intravenously injected into NSG mice via the tail vein, and lung metastasis burden was monitored after 19-22 days or 50 days, respectively, by IVIS in vivo bioluminescence imaging. $1x10^5$ A375 melanoma cells were subcutaneously injected into NSG mice, and spontaneous lung metastases were monitored after 28 days by IVIS in vivo bioluminescence imaging. For IVIS imaging, mice were anesthetized with isoflurane and then intraperitoneally injected with 100 µL Luciferin (4 mg/ml). Bioluminescent imaging was performed 10 min following Luciferin injection using the Xenogen IVIS Spectrum (Caliper Life Sciences). Mice were euthanized 3 days after IVIS imaging, and lungs were resected and fixed in Formalin. Tissue embedding in paraffin, sectioning, and H&E staining were performed by IDEXX. The quantification of lung metastasis tumor burden was performed with QuPath. ESC-GEMM chimeras were produced as previously described (Bok et al., 2019). Briefly, BP ES cells were targeted with the appropriate targeting vectors via

recombination-mediated cassette exchange by the Moffitt Gene Targeting Core. Targeting was verified by PCR, and at least two positive clones were injected into Balb/c blastocysts to produce chimeras. Tumor development was induced by administering 25 mg/ml 4OHT in DMSO to the shaved back skin with a paintbrush on 2 consecutive days at 3-4 weeks of age. BP ES cells are male, but the sex of blastocysts at the time of injection is not known. Thus, either male or hermaphroditic chimeras were used. Chimeras were placed on Doxycycline-containing chow (Envigo) immediately following 4OHT administration. Chimeras were euthanized when primary tumor size reached 1 mm^3.

METHOD DETAILS

TCGA data and ceRNA prediction

Copy number and expression data from 366 Skin Cutaneous Melanoma (SKCM) metastatic cases in The Cancer Genome Atlas was analyzed. Copy number variation determined by GISTIC 2.0 (-2 = homozygous deletion; -1 = hemizygous deletion; 0 = neutral / no change; 1 = gain; 2 = high level amplification) was downloaded from cBioPortal (http://www.cbioportal.org/). Gene expression quantified from RNA-seq (TPM values generated by RSEM) was downloaded from Broad Firehose website (https://gdac.broadinstitute.org/). Genes were ranked by average TPM values across 366 metastatic cases. A total of 211 genes with high level amplification in at least 3% cases and ranked within the top 20% highest expressed genes were further considered as ceRNA candidates. Spearman correlation was calculated between candidate ceRNAs and 20,291 protein-coding genes. ceRNA-gene pairs with Spearman correlation coefficient ≥0.5 and FDR adjusted P-value <0.05 were used for miRNA binding site prediction using TargetScan (Agarwal et al., 2015). A network was constructed with gene pairs sharing at least 4 miRNAs with aggregate P_{CT} score (Friedman et al., 2009) of ≥0.2 using R package network and visualized using R package ggnet2. Connectivity of the ceRNA nodes in the

network was evaluated using the Hyperlink-Induced Topic Search (HITS) algorithm implemented in R package networkR with default settings.

Gene set enrichment analysis

Global mRNA expression profiles of TCGA skin cutaneous melanoma dataset (TCGA-SKCM) were subject to GSEA to identify the association of *CEP170*, *NUCKS1*, and *ZC3H11A* with a melanoma metastasis gene signature (WINNEPENNINCKX_MELANOMA_METASTASIS_UP). For GSEA, expression of *CEP170*, *NUCKS1*, and *ZC3H11A* was used as phenotype, and "No_Collapse" was used for gene symbol. The metric for ranking genes in GSEA was set as 'Pearson', otherwise default parameters were used. GSEA was performed using GSEA 4.1.0 software.

Plasmid and lentivirus production

EGFP in pLenti-GFP-puro was removed with BamHI and SalI and replaced with the open reading frames (ORFs) of human *CEP170*, *NUCKS1*, *ZC3H11A*, or *AKT3*. The WPRE in pLenti-EGFP-blast, pLenti-EGFP-puro, or pLenti-EGFP-hygro was removed with SalI and EcoRI and replaced with the 3'UTRs of *CEP170*, *NUCKS1*, *ZC3H11A*, or *AKT3.* The sequences of shRNAs targeting *CEP170*, *NUCKS1*, or *ZC3H11A* were obtained from SplashRNA (http://splashrna.mskcc.org/) and cloned into pLenti-EGFP-miRE-puro using XhoI and EcoRI sites. To produce lentivirus supernatants, 6 µg of lentiviral vector along with 5.33 µg of Δ8.2 and 0.67 µg of VSVG helper plasmid were co-transfected into HEK293T Lenti-X cells in 10 cm dishes at 90% confluency. Lentiviral supernatant was collected 48 and 72 hours after tranfection, cleared using a 0.45 micron syringe filter, and used immediately to infect melanoma cells in the presence of 8 µg/ml polybrene or stocked in -80°C. Infected cells were selected with the appropriate antibiotics (1 µg/ml puromycin, 100 µg/ml hygromycin, or 10 µg/ml blasticidin) for 7 days.

Proliferation assay

800 A375 cells/well or 2,000 WM793 cells/well were plated in three 96 well plates in 100µL RPMI-1640 medium containing 5% FBS. Every other day, one plate was fized and stained cell with 50 µL crystal violet solution (0.5% crystal violet in 25% methanol) for 15 minutes. Crystal violet was discarded, and plates were gently washed twice with ddH_2O and air dried. 150 µl of 10% acetic acid was added per well to extract crystal violet. Absorbance of extracted crystal violet was measured at 600 nM using a Glomax microplate reader.

Soft agar assay

1.5% and 0.8% SeaPlaque Agarose in PBS solutions were made my microwaving. 1.5% agarose was mixed at a 1:1 ratio with RPMI-1640 medium to achieve 0.75% agarose, followed by plating 1 ml per well in a 12 well plate and letting agarose solidify at room temperature. Melanoma cells were trypsinized, counted and 500 cells were resuspended in 500 µl of RMPI-1640 medium containing 20% FBS. Cells were then mixed with 500 µl of 0.8% agarose (0.4% agarose and 10% FBS final concentrations) and plated atop the solidified 0.75% agar. Top layer was allowed to solidify at room temperature, followed by culture at 37°C with 100 µl of fresh medium added every 3 days. Pictures are taken after 10-15 days and analyzed with Image J.

Transwell migration and invasion assay

To pre-coated transwells with Matrigel, Matrigel was thawed on ice for at least 2 hours, diluted to 5% with ice-cold basic RPMI-1640 medium, and gently added to transwell inserts (50 µl/insert) and solidified at 37°C for 30 min. Melanoma cells were trypsinized and resuspend in RPMI-1640 medium. For transwell invasion assays, 5,000 A375 cells, 15,000 1205Lu cells, or 30,000 WM793 cells were plated per Matrigel-coated insert in 200 µl of RPMI-1640 without FBS. For transwell migration assay, 3,000 A375 cells, 10,000 1205Lu cells, or 20,000 WM793 cells were

plated per insert in 200 µl of RPMI-1640 without FBS. 500 µl RPMI-1640 medium containing 15% FBS were added into the bottom well. Plates were incubated at 37°C in a humidified incubator for 48 hr. Media was discarded, inserts were gently washed once with PBS, and cells were fixed with 500 µl fixing solution (ethanol:acetic acid = 3:1) in the bottom well outside the insert for 10 minutes. Inserts were washed once with PBS, and cells were stained in 500µL staining solution (0.5% crystal violet) for 30 minutes. Inserts were washed with tap water twice and non-migrated cells or Matrigel on the top side of the insert were carefully removed with cotton swabs, and inserts were air dried overnight. Pictures were taken at 200x magnification and cell numbers quantified.

miRNA reporter assay

Reverse complimentary sequences of candidate miRNAs (Table S2) were cloned into psiCHECK2 dual-luciferase reporter vector at the XhoI and NotI sites downstream of Renilla luciferase. $2x10^4$ cells/well were seeded in 96-well plates and allowed to settle for 24 hours. For each well of 96 well plate, 15 ng reporter plasmid were transfected using 0.5 µl Jetprime in 5 µL Jetprime buffer. 48 hr after transfection, cells were washed with PBS and lysed in 50 µl of lysis buffer (1x PLB, made from 5x PLB contained in the Dual Luciferase Reporter Assay System kit). Plates were rocked at room temperature for 15 min, and 20 µl of cell lysates were transferred to white-walled 96-well plates. Wash the injectors of the Glomax plate reader twice with ddH_2O, prime Injector 1 with buffer LAR II (for Firefly Luciferase) and prime Injector 2 with buffer STOP'n'GLO (for Renilla Luciferase, both contained in the Dual Luciferase Reporter Assay System kit). Set up the procedure for each well (Injector 1 volume: 50 µl, waiting duration: 2 seconds, reading integration: 5 seconds, Injector 2 volume: 50 µl, waiting duration: 2 seconds, reading integration: 5 seconds) then read the plate well by well in the luminometer automatically. Empty psiCHECK-2 control lacking MREs and appropriate vector or scramble controls were included in the experimental setup. Renilla luciferase values were normalized to Firefly

luciferase value to control for transfection efficiency. To analyze data, normalized Luciferase values of the MRE-bearing reporter were first compared to the empty reporter in vector or scramble control cells, and then the normalized Luciferase values of MRE-bearing reporter were compared to ceRNA overexpression or knockdown conditions.

RNA pulldown

Biotinylated oligonucleotide probes targeting GFP were designed using the online tool (https://www.biosearchtech.com/support/tools/design-software/chirp-probe-designer) and synthesized by Etonbio. $1x10^7$ cells were crosslinked using the UV cross-linker (Spectrolinker) with 600-1200J/cm^2. Cells were washed with PBS, collected in 1.5 ml tube, and lysed with 500-800 µl lysis buffer (TBS (pH7.4-7.6), 1 % Triton-X100, 0.1-0.5 % deoxycholate, 0.1-0.5 % SDS) containing 1% protease inhibitor cocktail and 0.1-0.5 % RNase inhibitor on ice for 15 min with repeated vortexing every 5 min. Lysates were cleared by centrifugation at 12,000g for 5 min at 4°C and transferred to new 1.5ml tubes. 100-200 µl of cell lysate were diluted 1:2 in hybridization buffer (500mM NaCl, 1% SDS, 100mM Tris (pH7.0), 10mM EDTA, 15% formamide). 1-2 nmol of probe mixture was added and mixed by end-to-end rotation at 37°C for 4 hours. Streptavidin beads were pre-cleared twice by adding 1 ml of hybridization buffer and collected using a magnetic rack. 20µl of Streptavidin beads were added per sample, mixed by end-to-end rotation at 37°C for 30 minutes, and washed 5 times in wash buffer for 5 minutes each at room temperature. Streptavidin beads were resuspended in 100 µl Proteinase K buffer (100mM Tris pH7.5, 200mM NaCl, 2mM EDTA, 1% SDS) containing Proteinase K (1 mg/ml), incubated at 55°C for 30 minutes, and boiled for 10 min. RNA was then isolated with the Qiagen miRNeasy kit.

miRNA mimics, miRNA inhibitors, Target Site Blockers (TSB)

miRNA mimics and miRNA inhibitors were purchased from Horizon Discovery and resuspended in ddH_2O to prepare 20μM solutions. miRNA mimics or miRNA inhibitors at 10 nM or 20 nM final concentration, respectively, were transfected into melanoma cells using JetPrime according to the manufacturer's recommendations. 48 hr after transfection, transwell invasion assays were performed or RNA was isolated.

Target Site Blockers: TSBs targeting the MREs of (i) miR-135, miR-141/200a, miR-144, or miR-203 on the *CEP170* 3'UTR; (ii) miR-135, miR-137, or miR-203 on the *NUCKS1* 3'UTR; and (iii) miR-101/137/144, or miR-200b/200c on the *ZC3H11A* 3'UTR were obtained from Qiagen. TSBs were resuspended in ddH_2O to prepare a 50 μM solution. TSBs were transfected into melanoma cells at a final concentration of 50nM. For xenograft metastasis assays, melanoma cells were intravenously injected into NSG mice 24 hr after TSB transfection. Transwell invasion assays were performed 48 hr after TSB transfection. RNA and protein were isolated 72 hr and 96 hr, respectively, after TSB transfection.

Droplet digital PCR (ddPCR)

RNA was isolated from 1x10^6 cells using Trizol using the manufacturer's recommendation. RNA was reverse transcribed into cDNA using the TaqMan MicroRNA Reverse Transcription Kit (Thermo Fisher Scientific) (miRNA) or PrimeScrip RT Master Mix (Takara) (mRNA). cDNA samples (10fg~100ng/reaction), Taqman probes (FAM, 20x), ddPCR supermix (2x) and ddH_2O were combined in a total volume of 22 μl in 96-well plates, and plates were sealed, centrifuged for 30 sec at 1,000rpm, and loaded into the Generator along with required consumables (DG32 cartridges, tips, waste bins, droplet plate, and oil) to partition the samples into droplets. Plates the containing droplets were sealed with foil, and PCR was performed to end point (~40 cycles) using the conditions outlined in Table S10. Plates were then loaded into the QX200 Reader to quantify positive and negative droplets in each sample and to plot fluorescence signal droplet by

droplet. Results are visualized in Quantasoft Software. The fraction of positive droplets in a sample determines the concentration of target in copies/µl.

qRT-PCR

RNA was extracted from cells using TRIzol (Invitrogen) following protocols supplied by the manufacturer. First-strand cDNA was generated with PrimeScript RT Master Mix (Takara). qPCR was performed on StepOnePlus™ Real-Time PCR System (Thermo Fisher), and PerfeCTa SYBR green Fastmix (Quantabio) was used for gene detection. The sequences of primers were obtained from PrimerBank (https://pga.mgh.harvard.edu/primerbank/index.html) and are listed in Table S2.

Western blot

15 µg of protein were loaded onto NuPAGE 4%-12% precast gels and separated by electrophoresis with NuPAGE running buffer at constant 120V for approximately 2 hr. Proteins were transferred to nitrocellulose membranes with transfer buffer at constant 300mA for 2 hr. Membranes were blocked in 5% non-fat dry milk solution in TBST for 30 min and then incubated with one of the following primary antibodies overnight at 4°C: anti-ZEB1 (1:1,000), anti-ZEB2 (1:1,000), anti-ROCK1 (1:1,000), anti-ROCK2 (1:1,000), anti-SP1 (1:1,000), anti-SUZ12 (1:1,000), or anti-BMI1 (1:1,000). Anti-beta-actin (1:3,000) was blotted as a loading control. Membranes were washed 3 times with TBST for 10 min, followed by incubation with HRP-conjugated secondary antibodies (1:2,000) for 1 hr room temperature. After three washes in TBST, chemiluminescence substrate (1:1) was applied to the blot for 4 min and chemiluminescence signal was captured using a LI-COR imaging system.

Quantification and statistical analysis

Proliferation assays are presented as mean ± SD. For soft agar, transwell migration, and invasion assays, 3 or 4 random fields were quantified for each well and data are presented as mean ± SEM. For luciferase reporter assays and RNA pulldown assays data are presented as mean ± SEM. Droplet digital PCR data were generated using 4 replicates and presented as mean ± SD. All experiments were performed at least 3 times with 3-4 technical replicates. Statistical analyses were performed by Student's unpaired t test. Data of in vivo imagining of lung metastasis are presented as mean ± SEM. Survival analysis of ESC-GEMMs was based on a cohort of 58 mice (22 TRE-GFP mice, 10 TRE-CEP170 mice, 11 TRE-NUCKS1 mice, and 15 TRE-ZC3H11A mice) and the p values were calculated based on a log-rank test. A p value of < 0.05 was considered statistically significant.

SUPPLEMENTAL TABLES

Supplemental Table S1: List of 211 candidate ceRNAs

Supplemental Table S2: List of miRNA families predicted for the candidate ceRNAs

Supplemental Table S3: List of ceRNA/effector gene pairs

Supplemental Table S4: HITS analysis

Supplemental Table S5: Luc-MRE reporter assay results for sponging of predicted miRNAs

Supplemental Table S6: List of validated pro-metastatic targets of sponged miRNAs

Supplemental Table S7: Log_2 fold change of expression of effectors upon ceRNA 3'UTR overexpression ± miRNA mimics

Supplemental Table S8: Log_2 fold change of expression of effectors upon ceRNA silencing ± miRNA inhibitors

Supplemental Table S9: Spearman correlations of $1q^{AMP}$ ceRNAs and effectors across 8 cancer types

Supplemental Table S10: qRT-PCR primer sequences, MRE reporter sequences, transfection conditions, ddPCR procedure

SUPPLEMENTAL FIGURE LEGENDS

Figure S1. CEP170, NUCKS1, and ZC3H11A, but not AKT3 and HNRNPU, are potential ceRNAs on chromosome 1q, related to Figure 1

(A) HITS score of the 40 predicted ceRNAs in melanoma.

(B) Number of overlapping effectors of the 40 predicted ceRNAs in melanoma. (C) Number of unique and overlapping effectors of the ceRNAs localized on chromosome 1q.

(D) Percentage Distal Usage Index (PDUI) scores of *AKT3*, *NUCKS1*, *HNRNPU*, *ZC3H11A*, and *CEP170*, the top ranked ceRNAs localized on chromosome 1q.

(E) Correlation between genomic alteration and gene expression of *CEP170*, *NUCKS1*, and *ZC3H11A*.

(F) Proliferation assay of A375 and WM793 cells overexpressing GFP-AKT3-3'UTR, the AKT3 coding sequence (CDS) or a GFP control.

In (E-G), N = 3 biological replicates; two-sided t test. Values represent mean ± SEM. ** $p < 0.01$, ns not significant.

(G) Anchorage-independent growth in soft agar of A375 and WM793 cells overexpressing the GFP-AKT3-3'UTR or a GFP control.

(H) Migration in a transwell assay of A375 and WM793 cells overexpressing the GFP-AKT3-3'UTR or a GFP control.

Figure S2. Quantification of $1q^{AMP}$ ceRNA overexpression and silencing, and effect of $1q^{AMP}$ ceRNA CDS on melanoma cell biology, related to Figure 2

(A) qRT-PCR showing the relative levels of the $1q^{AMP}$ ceRNAs 3'UTRs in WM793 and A375 cells expressing GFP-CEP170-3'UTR, GFP-NUCKS1-3'UTR, or GFP-ZC3H11A-3'UTR. Expression was normalized to the GFP control cells.

(B) qRT-PCR showing the knock down efficiency of *CEP170*, *NUCKS1*, or *ZC3H11A* in 1205Lu cells.

(C) Proliferation assays of A375 cells expressing GFP, the $1q^{AMP}$ ceRNA 3'UTRs (GFP-CEP170-3'UTR, GFP-NUCKS1-3'UTR, or GFP-ZC3H11A-3'UTR), or the $1q^{AMP}$ ceRNA CDS.

(D) Proliferation assays of WM793 cells expressing GFP, the $1q^{AMP}$ ceRNA 3'UTRs (GFP-CEP170-3'UTR, GFP-NUCKS1-3'UTR, or GFP-ZC3H11A-3'UTR), or the $1q^{AMP}$ ceRNA CDS.

(E) Anchorage-independent growth in soft agar of A375 and WM793 cells overexpressing the $1q^{AMP}$ ceRNA CDS. A representative image (*left*) and quantification (*right*) are shown.

(F) Quantification of transwell migration assay of A375 and WM793 cells overexpressing the $1q^{AMP}$ ceRNA CDS.

N = 3 biological replicates; two-sided t test. Values represent mean ± SEM. * $p < 0.05$, ** $p < 0.01$, *** $p < 0.001$, ns not significant.

Figure S3. $1q^{AMP}$ ceRNAs promote melanoma cell metastasis, related to Figure 3

(A) Quantification of lung metastasis burden in NSG mice subcutaneously transplanted with A375 cells expressing GFP or the $1q^{AMP}$ ceRNAs (GFP-CEP170-3'UTR, GFP-NUCKS1-3'UTR, GFP-ZC3H11A-3'UTR) individually or in combination.

(B) Quantification of lung metastasis burden in NSG mice intravenously transplanted with WM793 cells expressing GFP or the $1q^{AMP}$ ceRNAs (GFP-CEP170-3'UTR, GFP-NUCKS1-3'UTR, GFP-ZC3H11A-3'UTR) individually or in combination.

(C) Quantification of lung metastasis burden in NSG mice intravenously transplanted with 1205Lu cells expressing shRNAs against *CEP170*, *NUCKS1*, *ZC3H11A*, or a scrambled control.

(D-F) Representative images of bioluminescence imaging of the NSG mice shown in (A-C).

(G) Outline of the ESC-GEMMs approach.

N = 3 biological replicates; two-sided t test. Values represent mean ± SEM. * $p < 0.05$, ** $p < 0.01$, *** $p < 0.001$, ns not significant.

Figure S4. Identification of tumor suppressive miRNAs that are sequestered by the 1q^{AMP} ceRNAs, related to Figure 4

(A) Outline of the MRE luciferase reporter assay. MREs were cloned downstream of luciferase sequence, leading to repression by endogenous miRNAs. Co-expression of 1qAMP ceRNAs will result in de-repression of the reporter constructs.

(B) Outline of RNA pulldown assay. Biotinylated GFP probes were used to pull down GFP, GFP-CEP170-3'UTR, GFP-NUCKS1-3'UTR, and GFP-ZC3H11A-3'UTR with Streptavidin beads.

(C) Luciferase assays using dual luciferase reporters harboring MREs for miR-135-5p, miR-141-3p, miR-144-3p, miR-200-3p, or miR-203-3p in A375 cells expressing GFP or GFP-CEP170-3'UTR. Luciferase activity was normalized to the reporter without MRE (vector).

(D) Luciferase assays using dual luciferase reporters harboring MREs for miR-135-5p, miR-137, or miR-203-3p in A375 cells expressing GFP or GFP-NUCKS1-3'UTR. Luciferase activity was normalized to the reporter without MRE (vector).

In (B-D), asterisks (*, **) indicate comparison of Luc-MRE reporter vs. empty control Luc reporter (Vector) and pound symbols ($^{\#}$, $^{\#\#}$) indicate comparison of 3'UTR vs. GFP.

(E) Luciferase assays using dual luciferase reporters harboring MREs for miR-101-3p, miR-125-5p, miR-137, miR-144-3p, miR-200-3p, or miR-497-5p in A375 cells expressing GFP or GFP-ZC3H11A-3'UTR. Luciferase activity was normalized to the reporter without MRE (vector).

(F-G) Copy numbers of the indicated mature miRNAs and endogenous *CEP170*, *NUCKS1*, *ZC3H11A* in A375 (F) and WM793 (G) cells were quantified by Droplet Digital PCR.

(H) Quantification of transwell invasion assays with 1205Lu cells transfected with the indicated miRNA inhibitors.

(I) Expression of the indicated miRNAs in primary and metastatic melanoma samples in TCGA melanoma dataset.

In (B-D, H), N = 3 biological replicates. Two-sided t test; values represent mean ± SEM. * $p < 0.05$, ** $p < 0.01$, *** $p < 0.001$, $^{\#}$ $p < 0.05$, $^{\#\#}$ $p < 0.01$.

Figure S5. The oncogenic effect of the 1q^{AMP} ceRNAs depends on miRNA binding, related to Figure 5

(A) Western blot validates the siRNA-mediated silencing of Dicer in 1205Lu cells expressing 1q^{AMP} ceRNAs.

(B-D) Quantification of transwell invasion of A375 cells upon transfection with the indicated miRNA mimics. A375 cells were engineered to overexpress GFP, or wildtype or MRE-mutant GFP-CEP170-3'UTR (B), GFP-NUCKS1-3'UTR (C), or GFP-ZC3H11A-3'UTR (D). Asterisks indicate comparisons of GFP vs. 3'UTR-WT vs. 3'UTR-Mut and pound symbols indicate comparisons of miRNA mimics vs. scrambled control in GFP control samples (blue bars).

(E) qRT-PCR to assess restoration of 1q^{AMP} ceRNA expression upon wildtype or MRE-mutant GFP-CEP170-3'UTR, GFP-NUCKS1-3'UTR, or GFP-ZC3H11A-3'UTR expression in 1205Lu cells having silenced endogenous *CEP170*, *NUCKS1*, or *ZC3H11A*, respectively. Asterisks indicate comparisons of 3'UTR expression in 3'UTR-WT/Mut restored vs. ceRNA shRNA and pound symbols indicate comparison of ceRNA shRNA vs. shRNA control.

(F-H) Corresponding miRNA inhibitors and MRE Luciferase reporters were transfected in 1205Lu cells expressing shRNAs targeting the 1q^{AMP} ceRNAs. Luciferase activity normalized to a scrambled shRNA control is shown.

N = 3 biological replicates; two-sided t test. Values represent mean ± SEM. * $p < 0.05$, ** $p < 0.01$, *** $p < 0.001$, $^{\#}$ $p < 0.05$, $^{\#\#}$ $p < 0.01$, $^{\#\#\#}$ $p < 0.001$, ns not significant.

Figure S6. The 1q^{AMP} ceRNAs regulate expression of pro-metastatic effectors, related to Figure 6

(A) 301 metastasis associated genes are validated targets of one or more of the miRNAs sequestered by the 1q^{AMP} ceRNAs, based on published literature.

(B) The expression correlation between the 301 miRNA targets and *CEP170*, *NUCKS1*, or ZC3H11A in TCGA cutaneous melanoma dataset are shown. 72 genes are highly correlated (R>0.25) and are potential ceRNA effectors.

(C) Volcano plot showing the differential expression of potential ceRNA effectors in primary and metastatic melanoma samples in TCGA dataset. 49 potential effectors are significantly higher expressed in metastatic melanoma compared to primary melanoma.

(D) Venn diagram showing that expression of 24 out of 49 putative effector correlates with two or three of the $1q^{AMP}$ ceRNAs.

(E) qRT-PCR showing expression of the indicated effectors in WM793 melanoma cells engineered to overexpress GFP-CEP170-3'UTR, GFP-NUCKS1-3'UTR, or GFP-ZC3H11A-3'UTR.

(F) Western blot showing the protein expression of the indicated effectors in 1205Lu melanoma cells following treatment with TSBs.

REFERENCES

Ackermann, J., Frutschi, M., Kaloulis, K., McKee, T., Trumpp, A., and Beermann, F. (2005). Metastasizing melanoma formation caused by expression of activated N-RasQ61K on an INK4a-deficient background. Cancer Research *65*, 4005–4011.

Agarwal, V., Bell, G.W., Nam, J.-W., and Bartel, D.P. (2015). Predicting effective microRNA target sites in mammalian mRNAs. ELife *4*, 101.

Ala, U., Karreth, F.A., Bosia, C., Pagnani, A., Taulli, R., Léopold, V., Tay, Y., Provero, P., Zecchina, R., and Pandolfi, P.P. (2013). Integrated transcriptional and competitive endogenous RNA networks are cross-regulated in permissive molecular environments. Proceedings of the National Academy of Sciences of the United States of America *110*, 7154–7159.

Bastian, B.C., LeBoit, P.E., Hamm, H., Bröcker, E.B., and Pinkel, D. (1998). Chromosomal gains and losses in primary cutaneous melanomas detected by comparative genomic hybridization. Cancer Research *58*, 2170–2175.

Bok, I., Vera, O., Xu, X., Jasani, N., Nakamura, K., Reff, J., Nenci, A., Gonzalez, J.G., and Karreth, F.A. (2019). A versatile ES cell-based melanoma mouse modeling platform. Cancer Research *80*, canres.2924.2019-921.

Bosia, C., Pagnani, A., and Zecchina, R. (2013). Modelling Competing Endogenous RNA Networks. PloS One *8*, e66609.

Bosson, A.D., Zamudio, J.R., and Sharp, P.A. (2014). Endogenous miRNA and Target Concentrations Determine Susceptibility to Potential ceRNA Competition. Molecular Cell *56*, 347–359.

Caramel, J., Papadogeorgakis, E., Hill, L., Browne, G.J., Richard, G., Wierinckx, A., Saldanha, G., Osborne, J., Hutchinson, P., Tse, G., et al. (2013). A Switch in the Expression of Embryonic EMT-Inducers Drives the Development of Malignant Melanoma. Cancer Cell *24*, 466–480.

Chatterjee, A., Rodger, E.J., and Eccles, M.R. (2018). Epigenetic drivers of tumourigenesis and cancer metastasis. Seminars in Cancer Biology *51*, 149–159.

Chiu, H.-S., Martínez, M.R., Bansal, M., Subramanian, A., Golub, T.R., Yang, X., Sumazin, P., and Califano, A. (2017). High-throughput validation of ceRNA regulatory networks. Bmc Genomics *18*, 418.

Chiu, H.-S., Martínez, M.R., Komissarova, E.V., Llobet-Navas, D., Bansal, M., Paull, E.O., Silva, J., Yang, X., Sumazin, P., and Califano, A. (2018). The number of titrated microRNA species dictates ceRNA regulation. Nucleic Acids Research *136*, 215–4369.

Cho, J.H., Robinson, J.P., Arave, R.A., Burnett, W.J., Kircher, D.A., Chen, G., Davies, M.A., Grossmann, A.H., VanBrocklin, M.W., McMahon, M., et al. (2015). AKT1 Activation Promotes Development of Melanoma Metastases. Cell Reports *13*, 898–905.

Damsky, W.E., Curley, D.P., Santhanakrishnan, M., Rosenbaum, L.E., Platt, J.T., Rothberg, B.E.G., Taketo, M.M., Dankort, D., Rimm, D.L., McMahon, M., et al. (2011). β-catenin signaling controls metastasis in Braf-activated Pten-deficient melanomas. Cancer Cell *20*, 741–754.

Damsky, W.E., Theodosakis, N., and Bosenberg, M. (2014). Melanoma metastasis: new concepts and evolving paradigms. Oncogene *33*, 2413–2422.

Dankort, D., Curley, D.P., Cartlidge, R.A., Nelson, B., Karnezis, A.N., Damsky, W.E., You, M.J., DePinho, R.A., McMahon, M., and Bosenberg, M. (2009). Braf(V600E) cooperates with Pten loss to induce metastatic melanoma. Nature Genetics *41*, 544–552.

Denecker, G., Vandamme, N., Akay, Ö., Koludrovic, D., Taminau, J., Lemeire, K., Gheldof, A., Craene, B.D., Gele, M.V., Brochez, L., et al. (2014). Identification of a ZEB2-MITF-ZEB1 transcriptional network that controls melanogenesis and melanoma progression. Cell Death Differ *21*, 1250–1261.

Denzler, R., Agarwal, V., Stefano, J., Bartel, D.P., and Stoffel, M. (2014). Assessing the ceRNA hypothesis with quantitative measurements of miRNA and target abundance. Molecular Cell *54*, 766–776.

Denzler, R., McGeary, S.E., Title, A.C., Agarwal, V., Bartel, D.P., and Stoffel, M. (2016). Impact of MicroRNA Levels, Target-Site Complementarity, and Cooperativity on Competing Endogenous RNA-Regulated Gene Expression. Molecular Cell *64*, 565–579.

Ell, B., and Kang, Y. (2013). Transcriptional control of cancer metastasis. Trends in Cell Biology *23*, 603–611.

Figliuzzi, M., Marinari, E., and Martino, A.D. (2013). MicroRNAs as a selective channel of communication between competing RNAs: a steady-state theory. Biophysical Journal *104*, 1203–1213.

Fountain, J.W., Bale, S.J., Housman, D.E., and Dracopoli, N.C. (1990). Genetics of melanoma. Cancer Surveys *9*, 645–671.

Friedman, R.C., Farh, K.K.-H., Burge, C.B., and Bartel, D.P. (2009). Most mammalian mRNAs are conserved targets of microRNAs. Genome Research *19*, 92–105.

Gao, S., Cheng, C., Chen, H., Li, M., Liu, K., and Wang, G. (2016). IGF1 3′UTR functions as a ceRNA in promoting angiogenesis by sponging miR-29 family in osteosarcoma. J Mol Histol *47*, 135–143.

Gilot, D., Migault, M., Bachelot, L., Journé, F., Rogiers, A., Donnou-Fournet, E., Mogha, A., Mouchet, N., Pinel-Marie, M.-L., Mari, B., et al. (2017). A non-coding function of TYRP1 mRNA promotes melanoma growth. Nature Cell Biology *19*, 1348–1357.

Hausser, J., and Zavolan, M. (2014). Identification and consequences of miRNA-target interactions--beyond repression of gene expression. Nature Reviews. Genetics *15*, 599–612.

Hong, W., Ruan, H., Zhang, Z., Ye, Y., Liu, Y., Li, S., Jing, Y., Zhang, H., Diao, L., Liang, H., et al. (2019). APAatlas: decoding alternative polyadenylation across human tissues. Nucleic Acids Res *48*, D34–D39.

Jens, M., and Rajewsky, N. (2014). Competition between target sites of regulators shapes post-transcriptional gene regulation. Nature Reviews. Genetics.

Jeyapalan, Z., Deng, Z., Shatseva, T., Fang, L., He, C., and Yang, B.B. (2011). Expression of CD44 3'-untranslated region regulates endogenous microRNA functions in tumorigenesis and angiogenesis. Nucleic Acids Res *39*, 3026–3041.

Kapoor, A., Goldberg, M.S., Cumberland, L.K., Ratnakumar, K., Segura, M.F., Emanuel, P.O., Menendez, S., Vardabasso, C., Leroy, G., Vidal, C.I., et al. (2010). The histone variant macroH2A suppresses melanoma progression through regulation of CDK8. Nature *468*, 1105–1109.

Karras, P., Riveiro-Falkenbach, E., Cañón, E., Tejedo, C., Calvo, T.G., Martínez-Herranz, R., Alonso-Curbelo, D., Cifdaloz, M., Pérez-Guijarro, E., Gómez-López, G., et al. (2019). p62/SQSTM1 Fuels Melanoma Progression by Opposing mRNA Decay of a Selective Set of Pro-metastatic Factors. Cancer Cell *35*, 46-63.e10.

Karreth, F.A., and Pandolfi, P.P. (2013). ceRNA cross-talk in cancer: when ce-bling rivalries go awry. Cancer Discovery *3*, 1113–1121.

Karreth, F.A., Tay, Y., Perna, D., Ala, U., Tan, S.M., Rust, A.G., DeNicola, G., Webster, K.A., Weiss, D., Perez-Mancera, P.A., et al. (2011). In vivo identification of tumor- suppressive PTEN ceRNAs in an oncogenic BRAF-induced mouse model of melanoma. Cell *147*, 382–395.

Karreth, F.A., Reschke, M., Ruocco, A., Ng, C., Chapuy, B., Léopold, V., Sjoberg, M., Keane, T.M., Verma, A., Ala, U., et al. (2015). The BRAF pseudogene functions as a competitive endogenous RNA and induces lymphoma in vivo. Cell *161*, 319–332.

Marie, K.L., Sassano, A., Yang, H.H., Michalowski, A.M., Michael, H.T., Guo, T., Tsai, Y.C., Weissman, A.M., Lee, M.P., Jenkins, L.M., et al. (2020). Melanoblast transcriptome analysis reveals pathways promoting melanoma metastasis. Nature Communications *11*, 333–18.

Mertens, F., Johansson, B., Höglund, M., and Mitelman, F. (1997). Chromosomal imbalance maps of malignant solid tumors: a cytogenetic survey of 3185 neoplasms. Cancer Research *57*, 2765–2780.

Orgaz, J.L., and Sanz-Moreno, V. (2013). Emerging molecular targets in melanoma invasion and metastasis. Pigment Cell & Melanoma Research *26*, 39–57.

Otsuka, T., Takayama, H., Sharp, R., Celli, G., LaRochelle, W.J., Bottaro, D.P., Ellmore, N., Vieira, W., Owens, J.W., Anver, M., et al. (1998). c-Met autocrine activation induces development of malignant melanoma and acquisition of the metastatic phenotype. Cancer Research *58*, 5157–5167.

Pencheva, N., Tran, H., Buss, C., Huh, D., Drobnjak, M., Busam, K., and Tavazoie, S.F. (2012). Convergent multi-miRNA targeting of ApoE drives LRP1/LRP8-dependent melanoma metastasis and angiogenesis. Cell *151*, 1068–1082.

Poliseno, L., Salmena, L., Zhang, J., Carver, B., Haveman, W.J., and Pandolfi, P.P. (2010). A coding-independent function of gene and pseudogene mRNAs regulates tumour biology. Nature *465*, 1033–1038.

Powers, J.T., Tsanov, K.M., Pearson, D.S., Roels, F., Spina, C.S., Ebright, R., Seligson, M., Soysa, Y. de, Cahan, P., Theißen, J., et al. (2016). Multiple mechanisms disrupt the let-7 microRNA family in neuroblastoma. Nature *535*, 246–251.

Rutnam, Z.J., and Yang, B.B. (2012). The non-coding 3′ UTR of CD44 induces metastasis by regulating extracellular matrix functions. J Cell Sci *125*, 2075–2085.

Salmena, L., Poliseno, L., Tay, Y., Kats, L., and Pandolfi, P.P. (2011). A ceRNA hypothesis: the Rosetta Stone of a hidden RNA language? Cell *146*, 353–358.

Shain, A.H., Joseph, N.M., Yu, R., Benhamida, J., Liu, S., Prow, T., Ruben, B., North, J., Pincus, L., Yeh, I., et al. (2018). Genomic and Transcriptomic Analysis Reveals Incremental Disruption of Key Signaling Pathways during Melanoma Evolution. Cancer Cell *34*, 45-55.e4.

Smillie, C.L., Sirey, T., and Ponting, C.P. (2018). Complexities of post-transcriptional regulation and the modeling of ceRNA crosstalk. Critical Reviews in Biochemistry and Molecular Biology *53*, 1–15.

Sumazin, P., Yang, X., Chiu, H.-S., Chung, W.-J., Iyer, A., Llobet-Navas, D., Rajbhandari, P., Bansal, M., Guarnieri, P., Silva, J., et al. (2011). An extensive microRNA-mediated network of RNA-RNA interactions regulates established oncogenic pathways in glioblastoma. Cell *147*, 370–381.

Tay, Y., Kats, L., Salmena, L., Weiss, D., Tan, S.M., Ala, U., Karreth, F., Poliseno, L., Provero, P., Cunto, F.D., et al. (2011). Coding-independent regulation of the tumor suppressor PTEN by competing endogenous mRNAs. Cell *147*, 344–357.

Tay, Y., Rinn, J., and Pandolfi, P.P. (2014). The multilayered complexity of ceRNA crosstalk and competition. Nature *505*, 344–352.

Thompson, F.H., Emerson, J., Olson, S., Weinstein, R., Leavitt, S.A., Leong, S.P., Emerson, S., Trent, J.M., Nelson, M.A., and Salmon, S.E. (1995). Cytogenetics of 158 patients with regional or disseminated melanoma. Subset analysis of near-diploid and simple karyotypes. Cancer Genetics and Cytogenetics *83*, 93–104.

Turner, N., Ware, O., and Bosenberg, M. (2018). Genetics of metastasis: melanoma and other cancers. Clinical & Experimental Metastasis *35*, 379–391.

Vandamme, N., Denecker, G., Bruneel, K., Blancke, G., Akay, Ö., Taminau, J., Coninck, J.D., Smedt, E.D., Skrypek, N., Loocke, W.V., et al. (2020). The EMT Transcription Factor ZEB2

Promotes Proliferation of Primary and Metastatic Melanoma While Suppressing an Invasive, Mesenchymal-Like Phenotype. Cancer Res *80*, 2983–2995.

Vogelstein, B., Papadopoulos, N., Velculescu, V.E., Zhou, S., Diaz, L.A., and Kinzler, K.W. (2013). Cancer genome landscapes. Science (New York, N.Y.) *339*, 1546–1558.

Wurth, L., Papasaikas, P., Olmeda, D., Bley, N., Calvo, G.T., Guerrero, S., Cerezo-Wallis, D., Martinez-Useros, J., García-Fernández, M., Hüttelmaier, S., et al. (2016). UNR/CSDE1 Drives a Post-transcriptional Program to Promote Melanoma Invasion and Metastasis. Cancer Cell *30*, 694–707.

Zingg, D., Debbache, J., Peña-Hernández, R., Antunes, A.T., Schaefer, S.M., Cheng, P.F., Zimmerli, D., Haeusel, J., Calçada, R.R., Tuncer, E., et al. (2018). EZH2-Mediated Primary Cilium Deconstruction Drives Metastatic Melanoma Formation. Cancer Cell *34*, 69-84.e14.

A

B

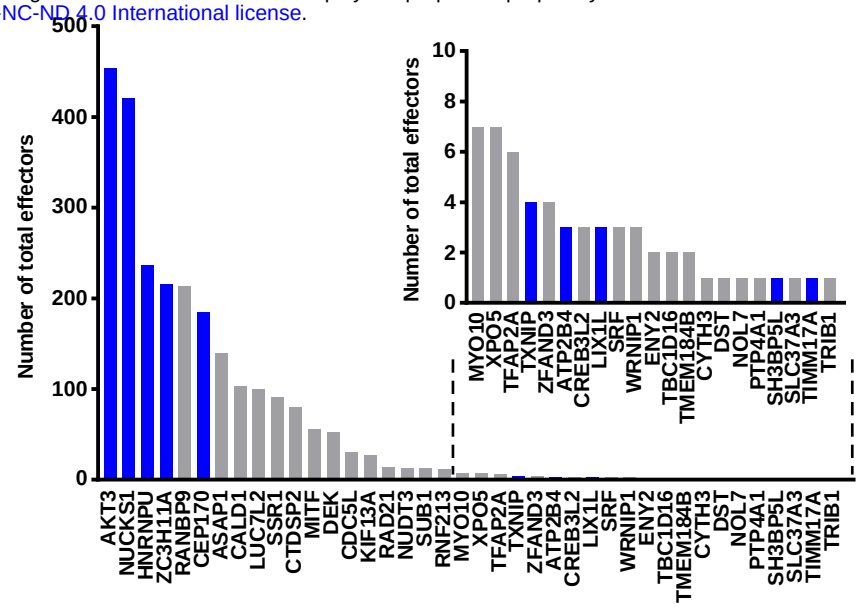

C

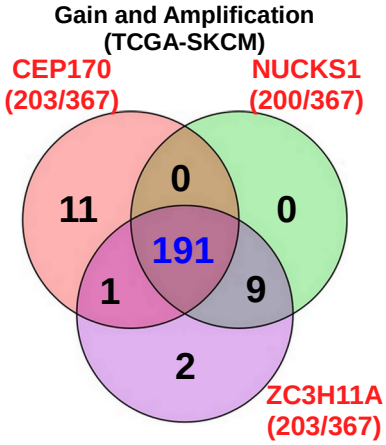

D

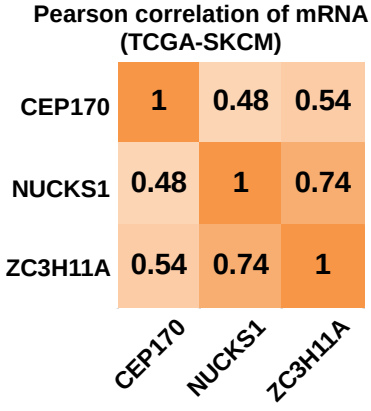

E

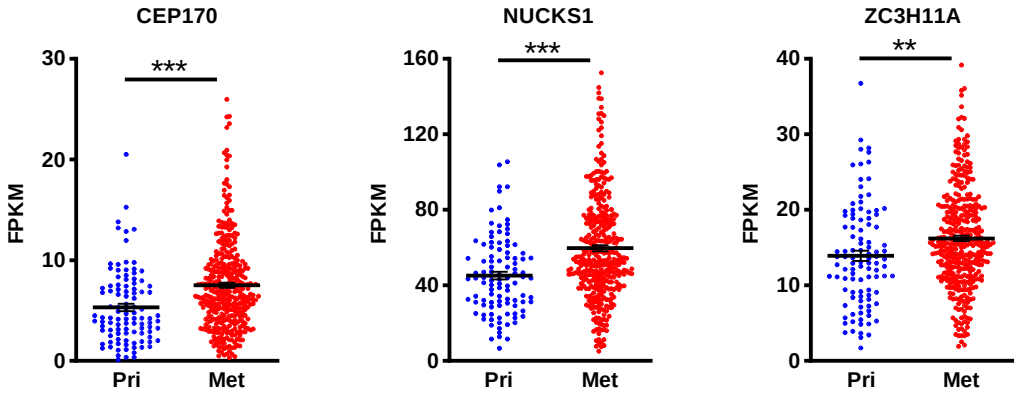

F

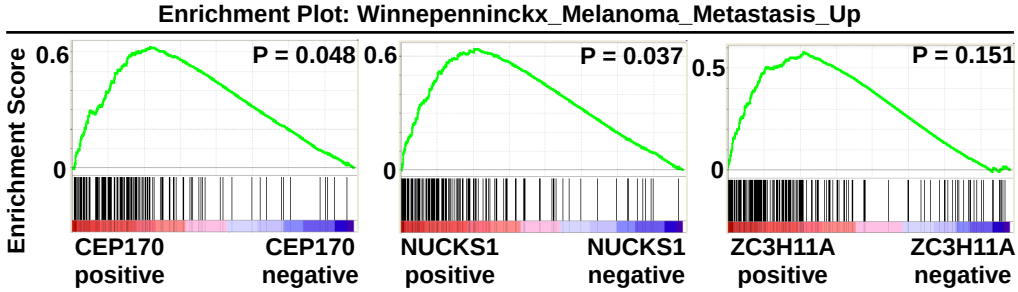

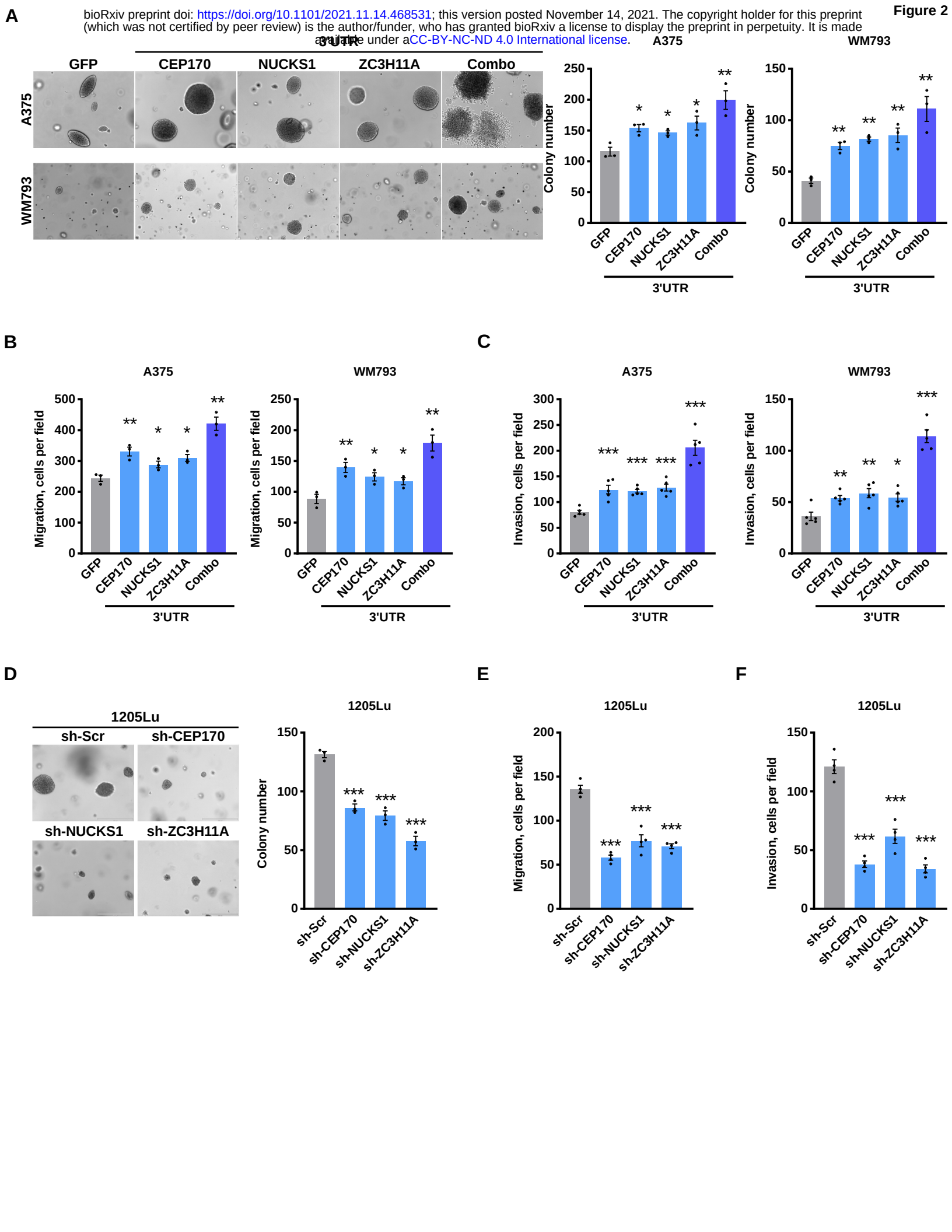

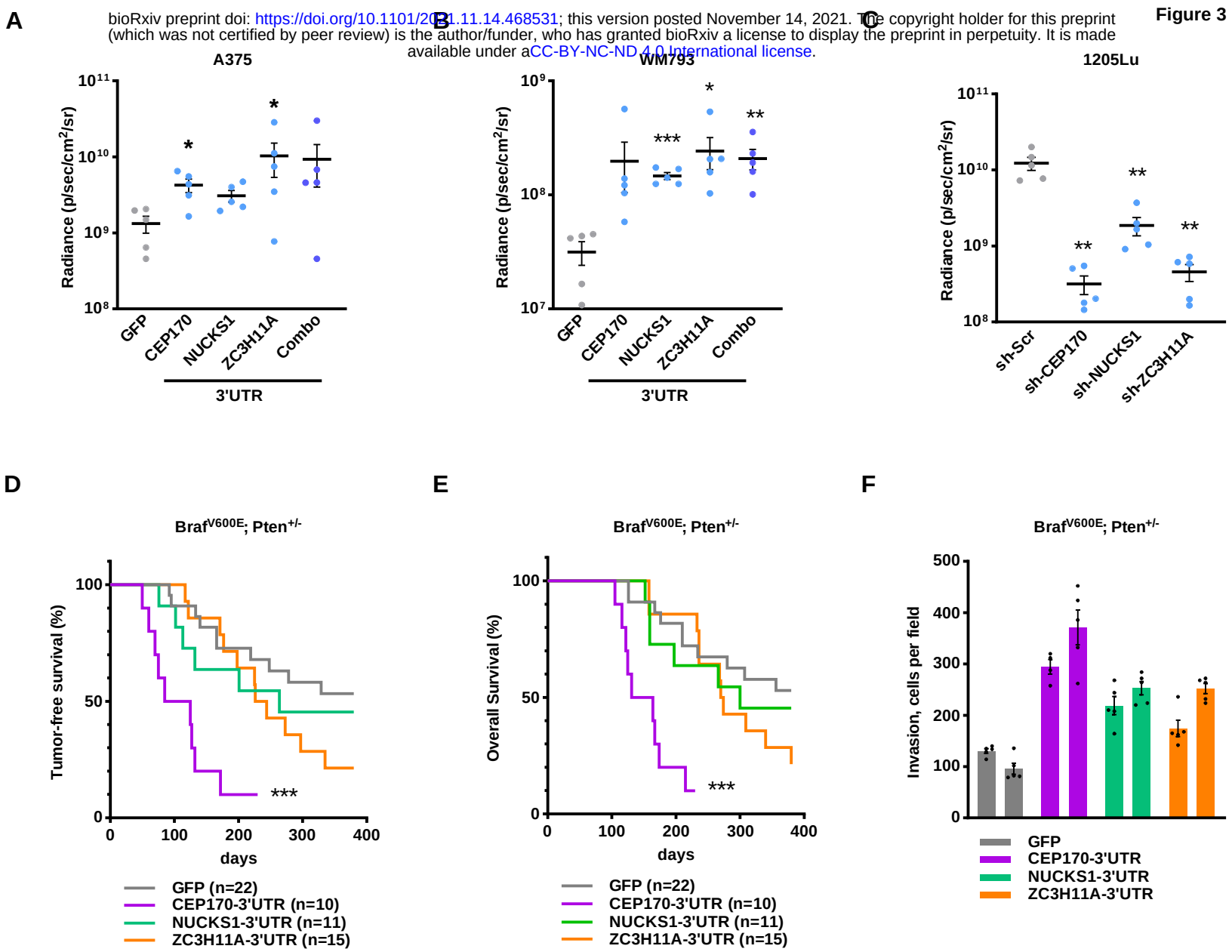

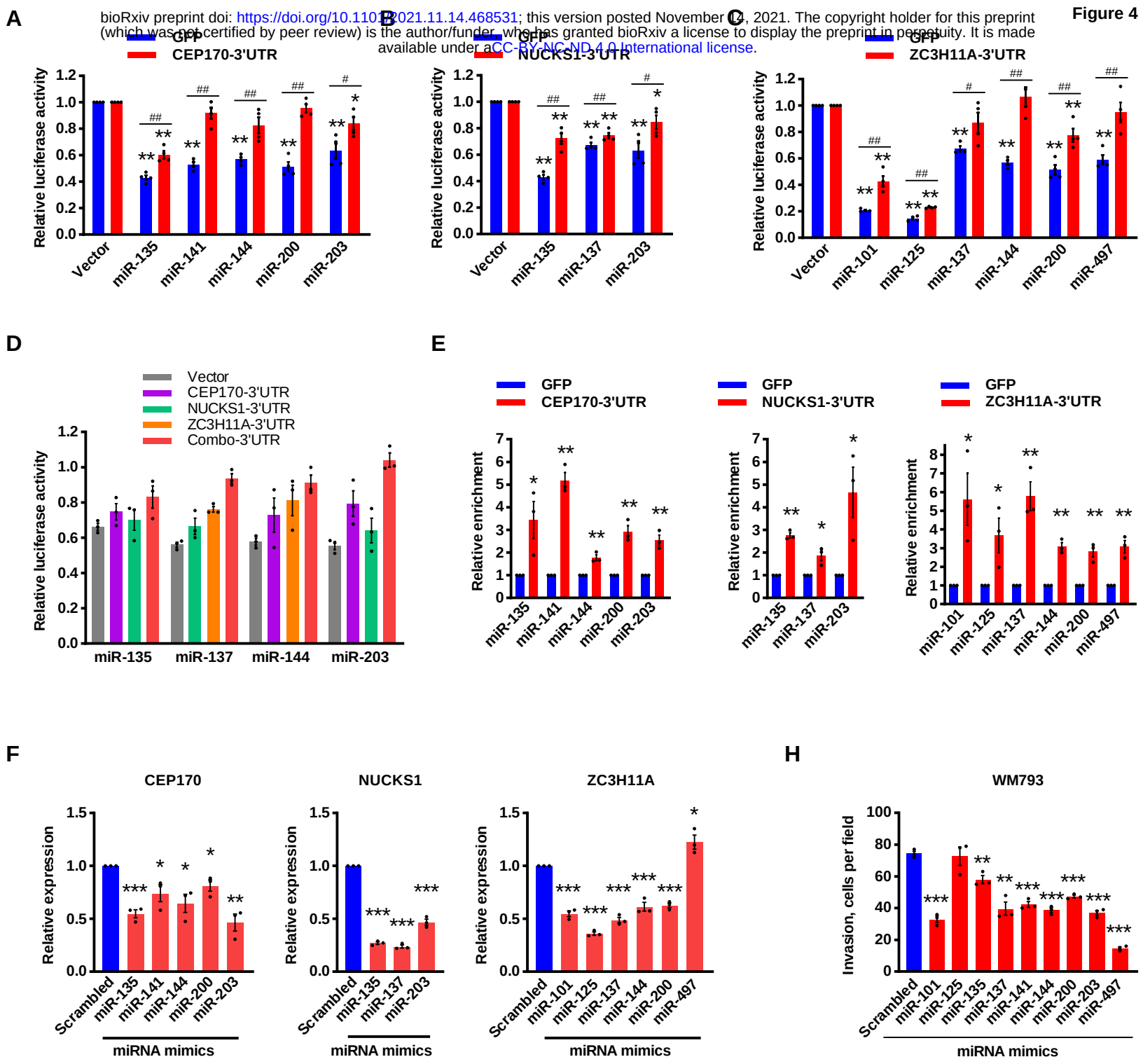

G

A375	miRNA (copies/ng)	MRE (copies/ng)
miR-101	908±33	1195±300
miR-125	57600±3934	1195±300
miR-135	730±40	5867±962
miR-137	547±17	6537±1124
miR-141	30±1.6	526±138
miR-144	3.7±1.6	1721±438
miR-200b	31.4±1.2	1195±300
miR-200c	100±7.5	1195±300
miR-203	9.2±1.8	5867±962
miR-497	42.6±3.3	1195±300

WM793	miRNA (copies/ng)	MRE (copies/ng)
miR-101	409±35	395±82
miR-125	58200±5786	395±82
miR-135	896±96	3003±829
miR-137	627±81	3181±854
miR-141	25±1.5	217±57
miR-144	5.1±2.1	613±139
miR-200b	35.6±2.1	395±82
miR-200c	86±3.9	395±82
miR-203	7.2±3.1	3003±829
miR-497	7.6±0.9	395±82

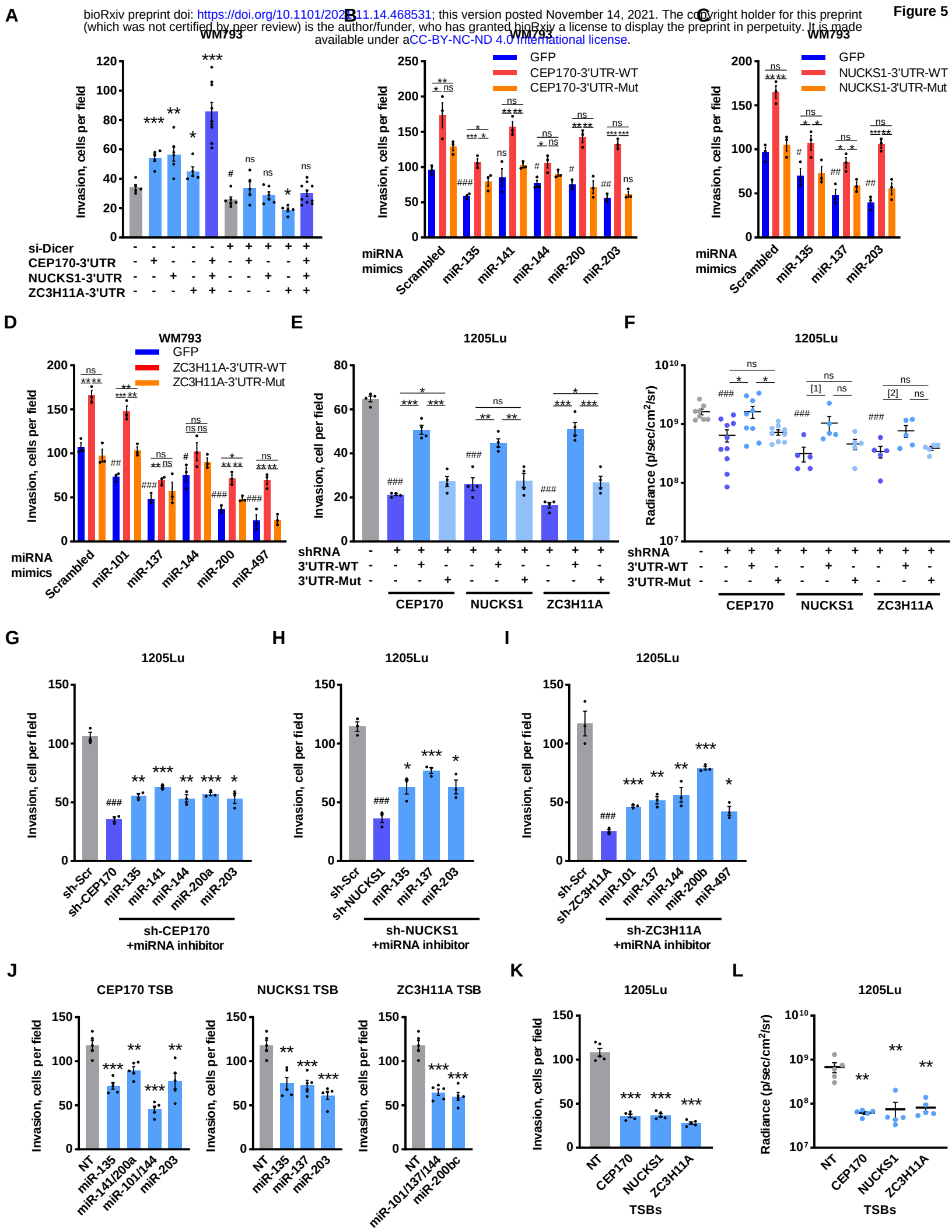

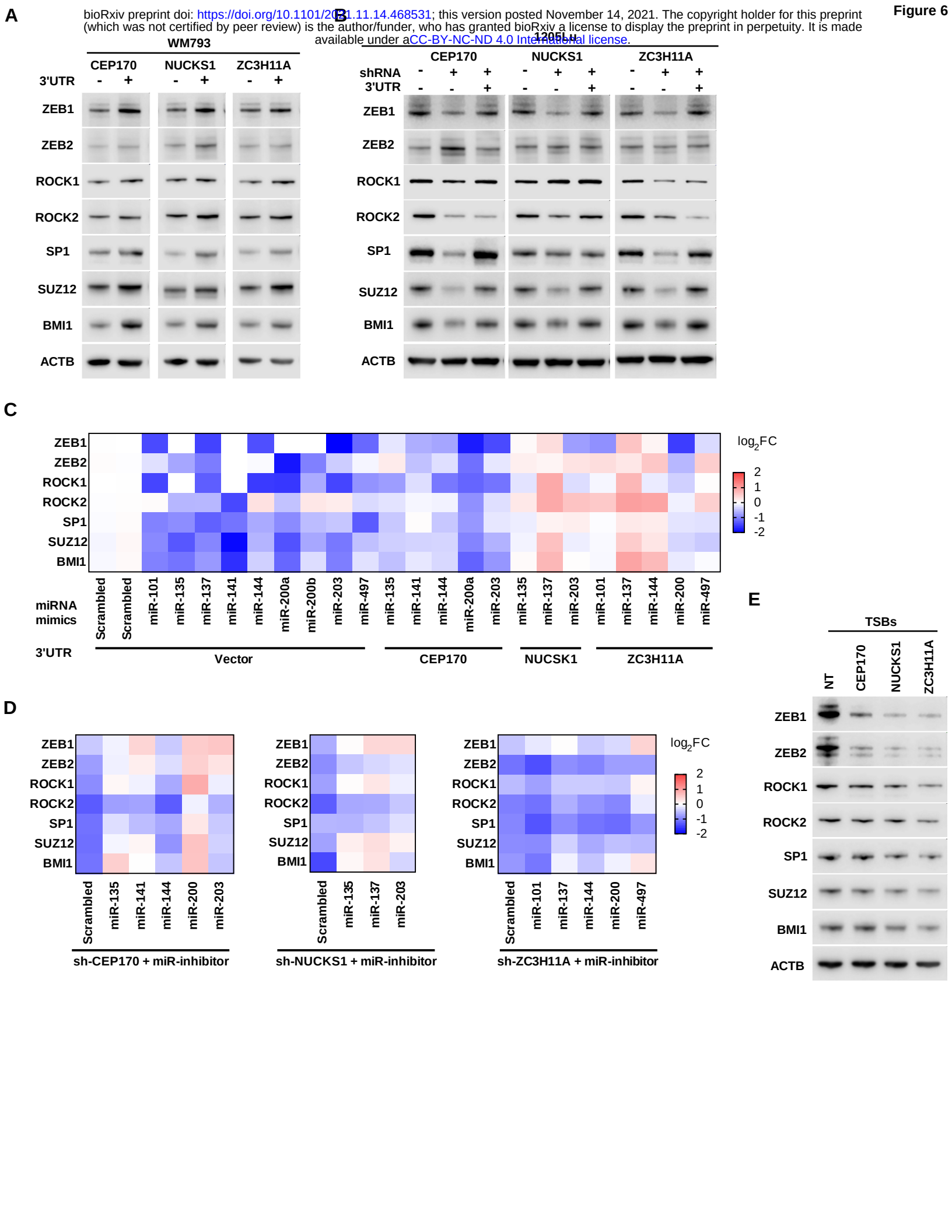

A

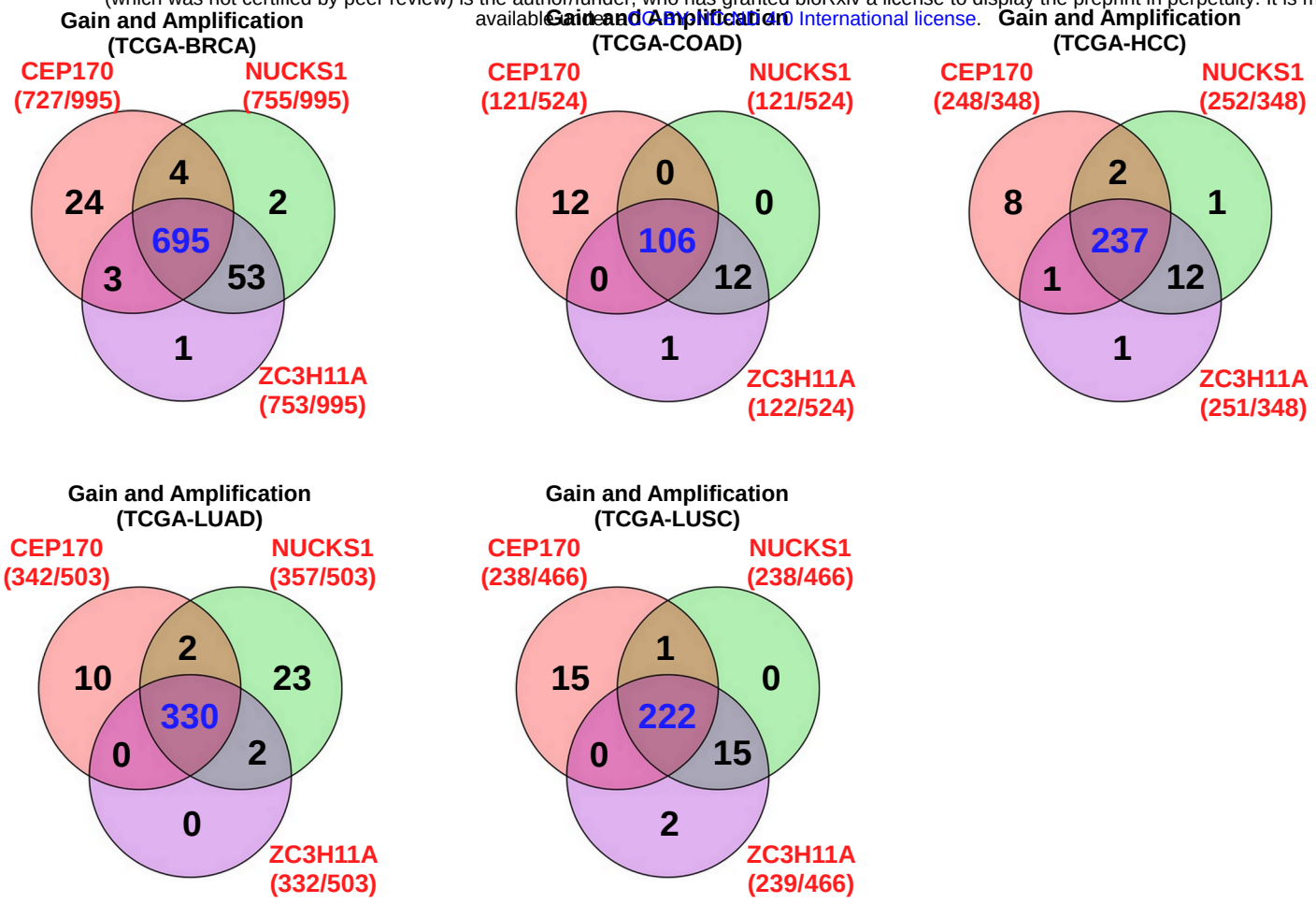

B

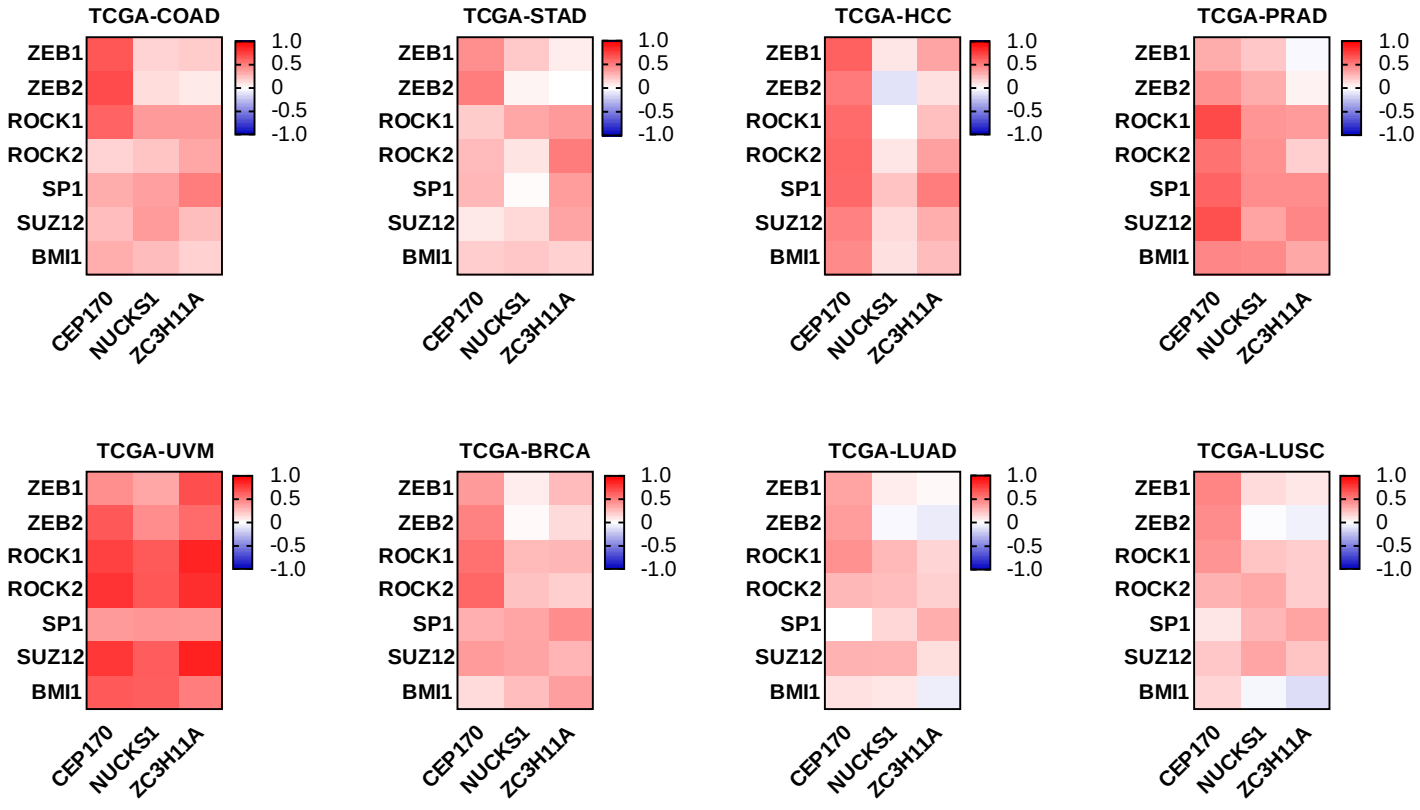

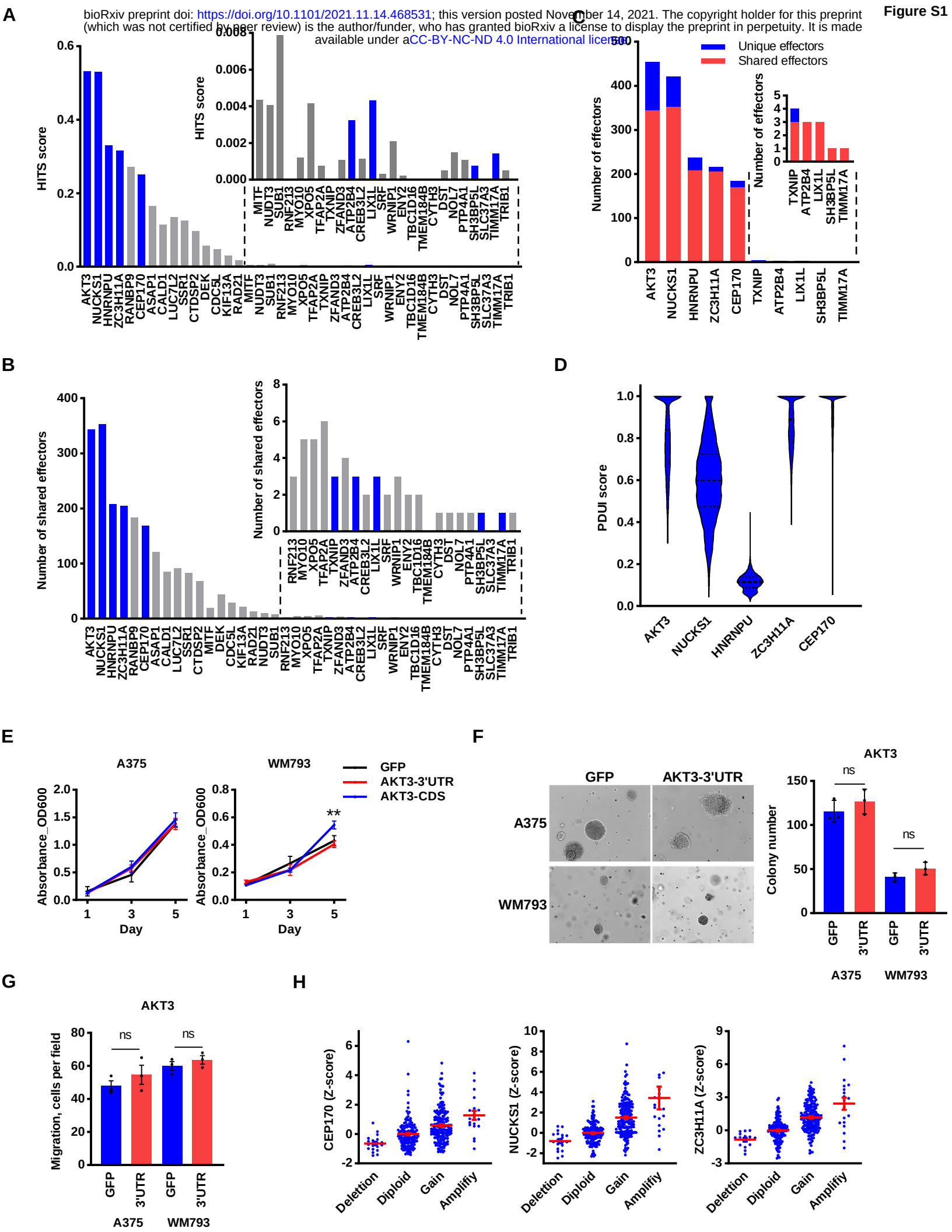

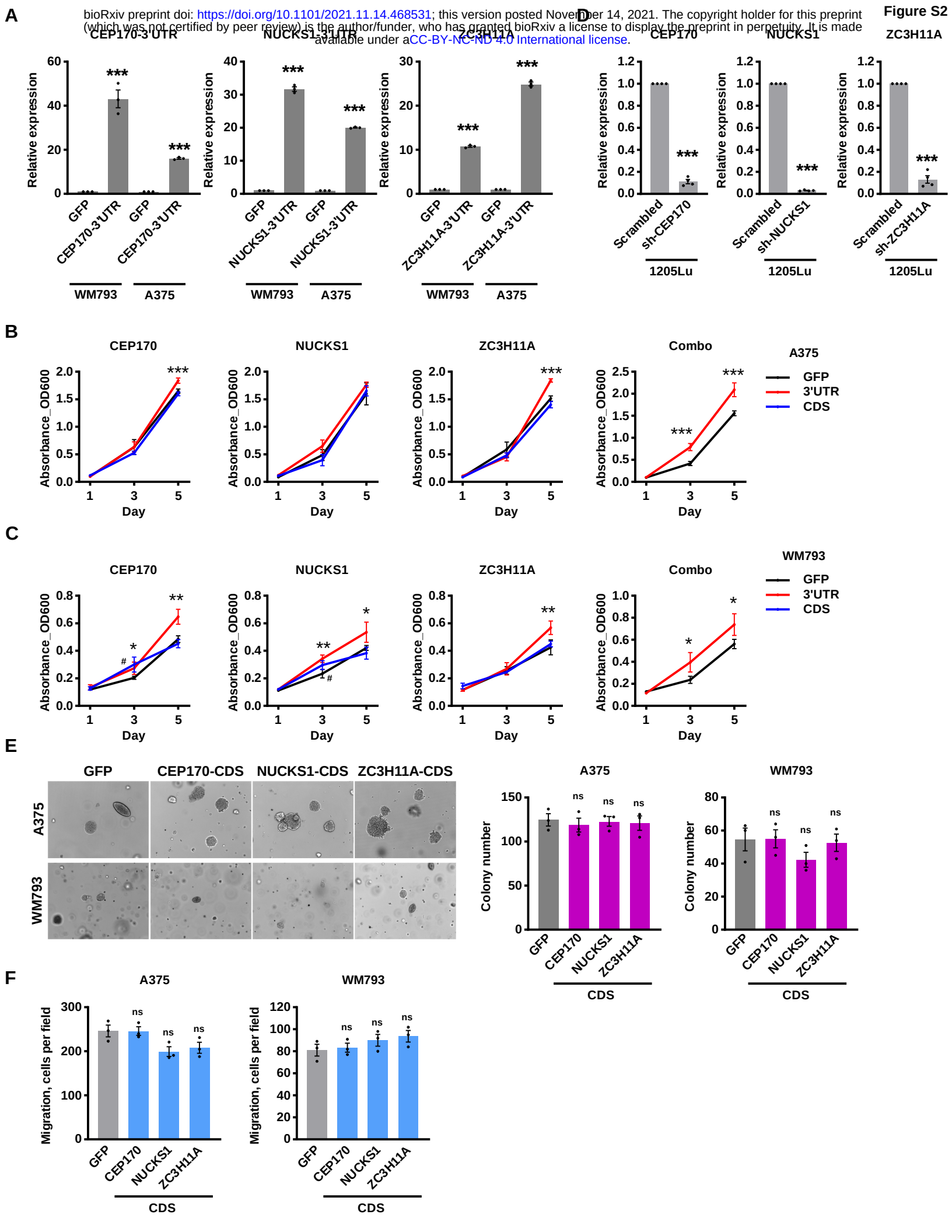

A

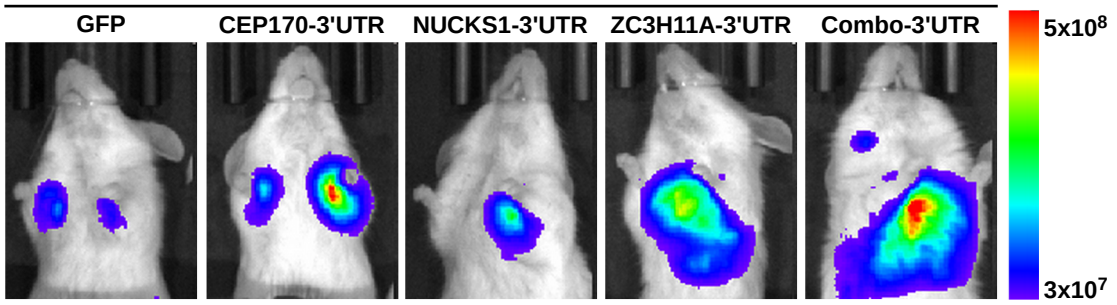

C

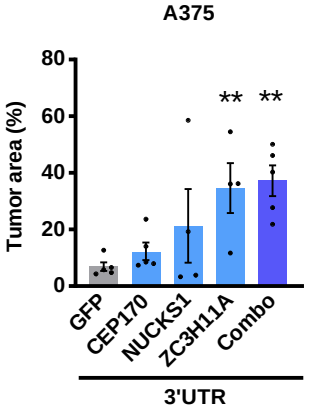

B

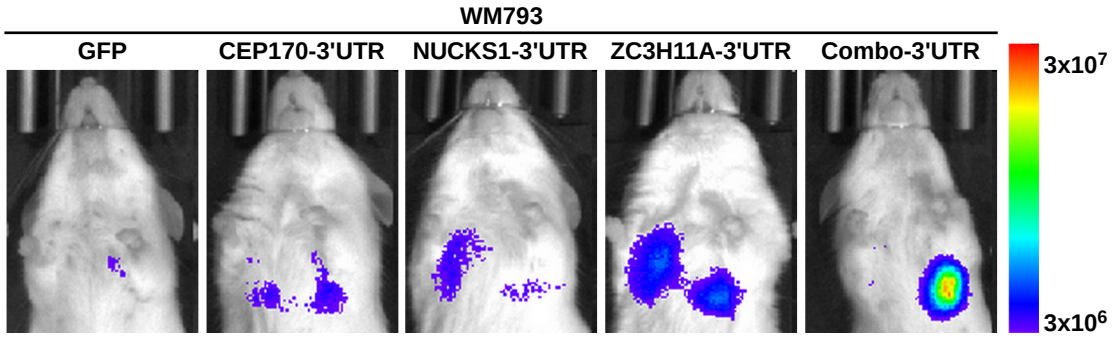

D

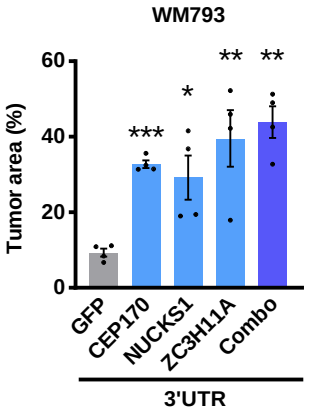

E

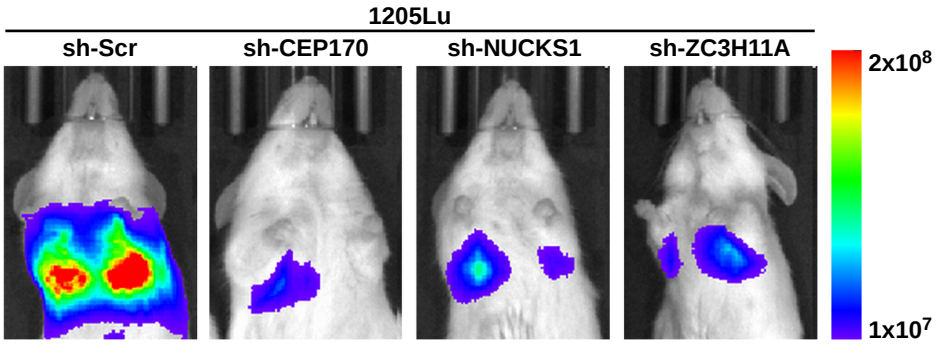

F

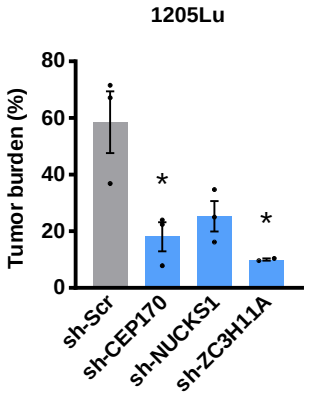

G

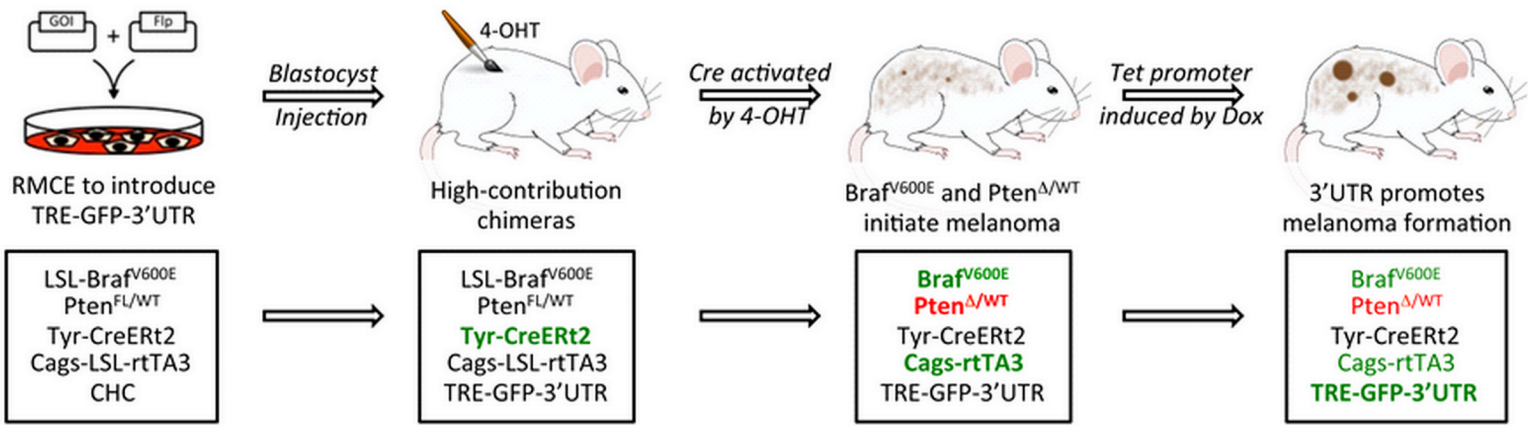

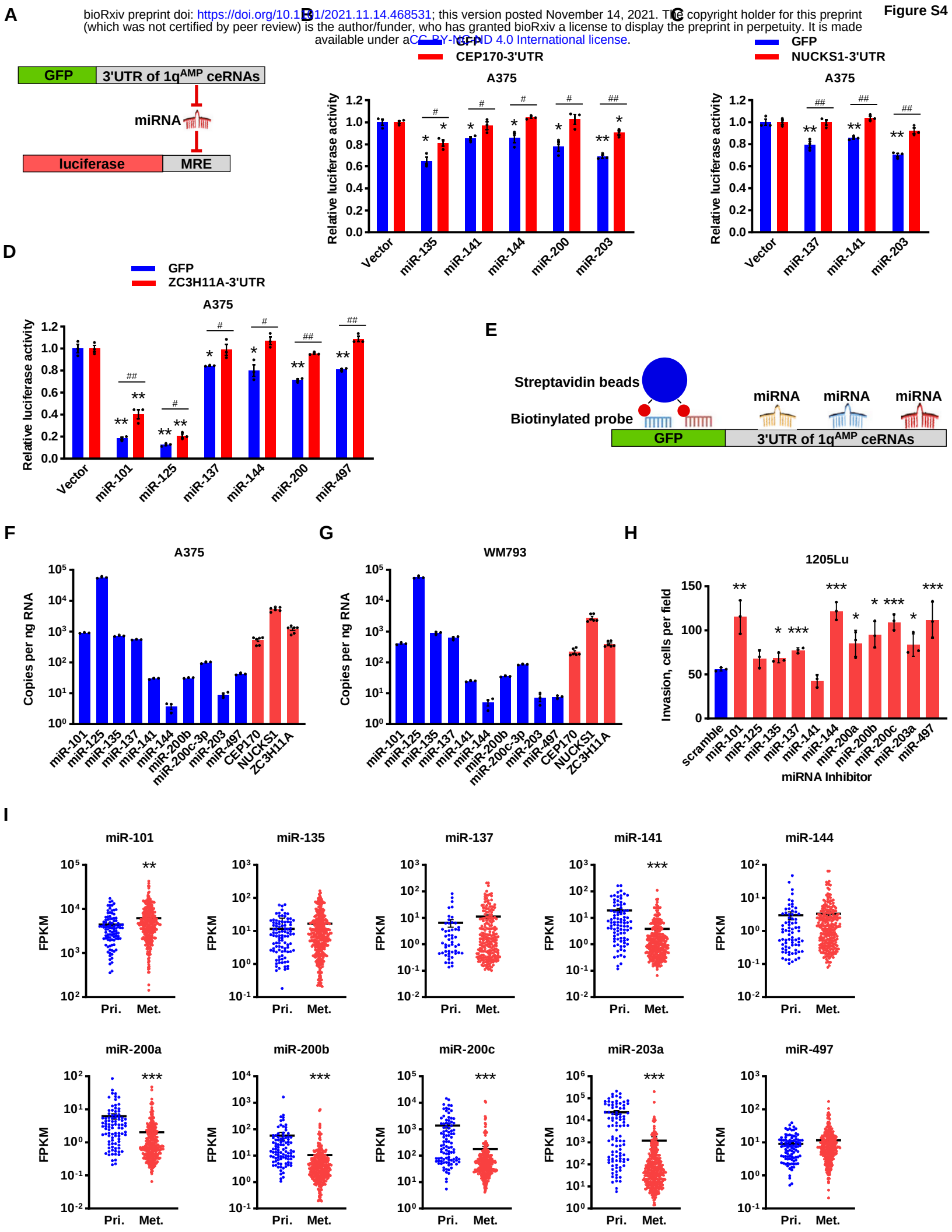

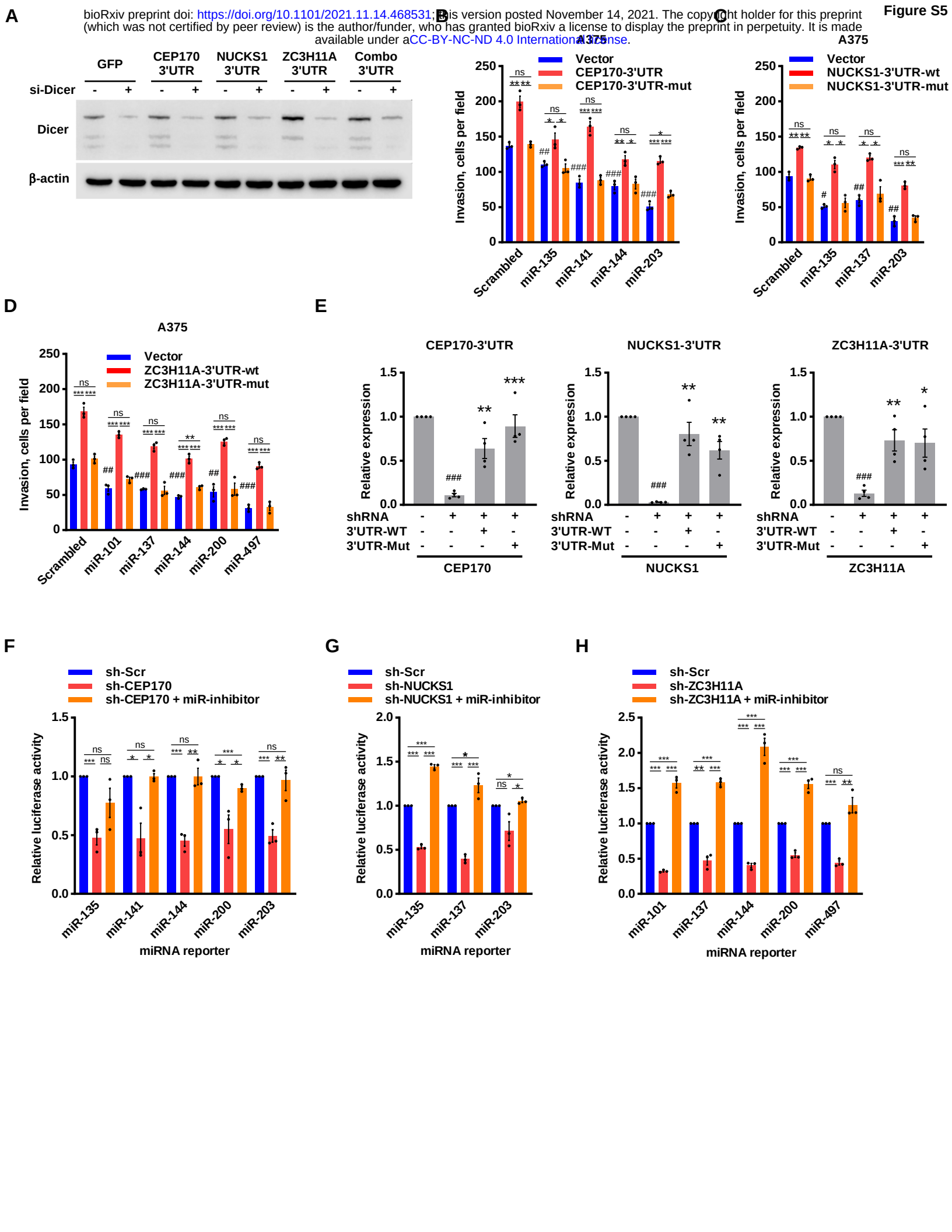

A

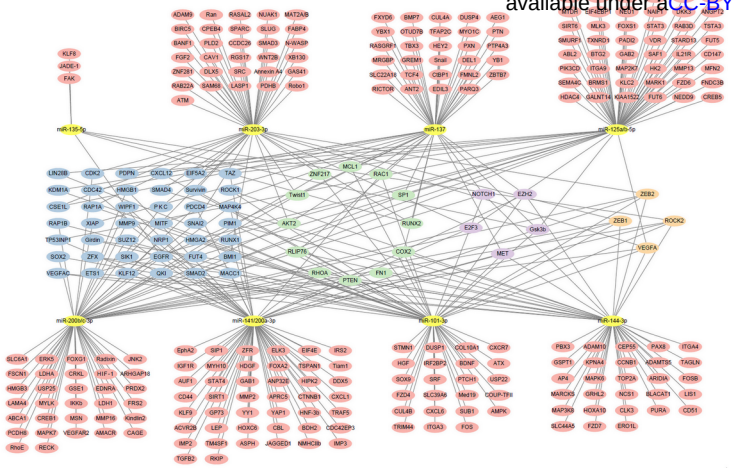

B

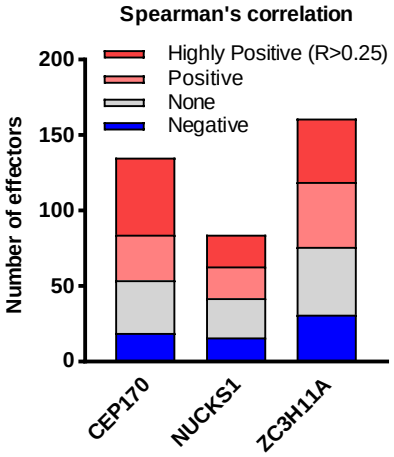

C

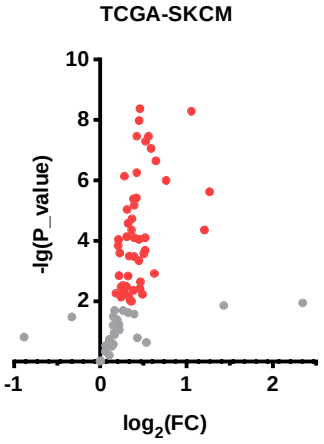

D

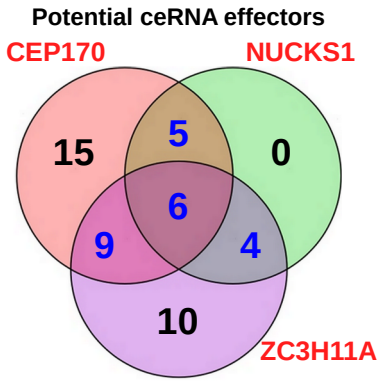

E

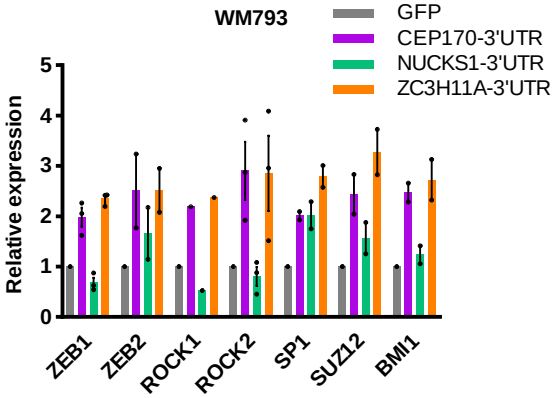

F